

Specificity of spatio-temporal order  
under rhythmic environmental parameter:  
Cooperation of real-world experiments with  
numerical modeling

UENO Hiroshi  
Doshisha University  
Graduate School of Life and Medical Sciences

10th June 2021

Doshisha University

Faculty of Life and Medical Sciences

ABSTRACT

Specificity of spatio-temporal order  
under rhythmic environmental parameter:

Cooperation of real-world experiments with numerical modeling

UENO Hiroshi

Supervisor: Professor OE Yohei

Many physical, chemical and biological systems exhibit a cooperative or sigmoidal response with respect to the input. In biochemistry, such behavior is called an allosteric effect. Here we demonstrate that a system with such properties can be used to discriminate the amplitude or frequency of an external periodic perturbation or input. Numerical simulations performed for a model sigmoidal kinetics illustrate that there exists a narrow range of frequencies and amplitudes within which the system evolves toward significantly different states. Therefore, observation of system evolution should provide information about the characteristics of the perturbation. The discrimination properties for periodic perturbation are generic. They can be observed in various dynamical systems and for different types of periodic perturbation.

Functionality of living organisms is based on decision making. Chemical reactions stand behind information processing in biological systems. Therefore, it is interesting to consider reaction models that show ability to make decisions by evolving towards significantly different states, depending on conditions at which those reactions proceed. It has been recently demonstrated that a system exhibiting cooperative or sigmoidal response with respect to the input can be used as a discriminator of the amplitude or the frequency of its external periodic perturbation. Here we consider a few models of allosteric enzymatic reactions and discuss their applicability for sensing the frequency or the amplitude of the reagent inflow. On the basis of numerical simulations we compare results for a full reaction model with its reduced, easier to analyze version.

Drying of an aqueous suspension containing fine granules leads to the formation of a circular pattern, i.e., the coffee-ring effect. Here, we report the effect of mechanical rotation with drying of an aqueous suspension containing a large amount of granular particles as in the Turkish coffee. It was found that wavy fragmented stripes, or a “waggly pattern”, appear in the early stage of the drying process and a “polka-dot pattern” with many small circles is generated in the late stage. We discuss the mechanism of these patterns in terms of the kinetic effect on micro phase-segregation. We suggest that the waggly pattern is induced through a mechanism similar to spinodal decomposition, whereas polka-dot formation is accompanied by the enhanced segregation of a water-rich phase under mechanical rotation.

This thesis is based on the following original papers and a book section. The chapters which include the contents of the articles are indicated:

Chapter 2 [1] <sup>\*1</sup>

Chapter 3 [2]

Chapter 4 [3]

## Publications

<sup>1</sup>H. Ueno, T. Tsuruyama, B. Nowakowski, J. Górecki and K. Yoshikawa, ‘Discrimination of time-dependent inflow properties with a cooperative dynamical system’, *Chaos: An Interdisciplinary Journal of Nonlinear Science* **25**, 103115 (2015).

<sup>2</sup>J. Gorecki, J. N. Gorecka, B. Nowakowski, H. Ueno, T. Tsuruyama and K. Yoshikawa, ‘Sensing Parameters of a Time Dependent Inflow with an Enzymatic Reaction’, in *Advances in Unconventional Computing: Volume 2: Prototypes, Models and Algorithms*, edited by A. Adamatzky, Emergence, Complexity and Computation (Springer International Publishing, Cham, 2017), pp. 85–104.

<sup>3</sup>H. Ueno, M. Shono, M. Ogawa, K. Sadakane and K. Yoshikawa, ‘Emergence of Many Mini-Circles from a Coffee Suspension with Mechanical Rotation’, *Physics* **3**, 10.3390/physics3010003 (2021).

---

<sup>\*1</sup> Reproduced from [1], with the permission of AIP Publishing

## Acknowledgements

First and foremost the author would like to acknowledge his past supervisor, Professor YOSHIKAWA Kenichi, for his support throughout his whole years in university and beyond. The author, who went through even the severe depression after entering university, has survived it by a great chance to encounter Professor OMIYA Mayumi, who passed recently, but introduced him to his professor, and live ever afterward at least as happily as their unafflicted counterparts\*<sup>2</sup>.

The author is also grateful to his supervisor, Professor OE Yohei and Professor OTA Tetsuo, without whose gentle questions and suggestions for this thesis the author could not serve it. The author never forget requital of the favour, continuous support and humour of his second supervisor, Assoc. Professor SADAKANE Koichiro.

His sincere gratitude goes to Professor KAWAKAMI Hiroshi from Tokushima University for offering the author the opportunity to discuss many things, the scientific atmosphere during his stay.

The author would like to express his sincere thanks to Professor Jerzy GÓRECKI from Institute of Physical Chemistry, Polish Academy of Sciences for inviting him to his group and for his hospitality and support during his stay in Warsaw, Poland.

The author would like to express his gratitude to his colleagues and friends from the laboratory, especially Dr. SAKUTA Hiroki, Mr. ODA Sotaro and Mr. NAKATANI Naoki for inspiring discussions and their valuable comments. The author is very grateful to Dr. TAKATORI Satoshi for his advises and help in experimental works and to Ms. FURUMOTO Makiko, the secretary of Professor Yoshikawa, for her perfect managements of paper works and her rejoicing activities in the laboratory. And also the author appreciates daily conversations and chatting with Ms. HASEGAWA Yoshino, Mr. NAKANISHI Tokuchiro, and Mr. NAKAJIMA Kazuma et al. during these difficult time

---

\*<sup>2</sup> William Styron, *Darkness Visible: A Memoir of Madness*, (Vintage, New York, 1992).

for all of us due to the situation with COVID-19.

The author rejoices in thoughtful help of Dr. IWAMURA Fumihiro, who dialogued often with him about the philosophical aspects of this thesis.

The author would like to express his special thanks also to Yoshida Scholarship Foundation for their financial and warm supports during master course and doctoral course. Without them, the author would have survived more hardly. They have enabled the author to concentrate on studies.

Finally, and most importantly, the author would like to thank his parents and the whole family for their understanding and endless support.

# Contents

Chapter 1	General Introduction	11
1.1	Introduction . . . . .	11
1.2	Backgrounds . . . . .	13
Chapter 2	Discrimination of time-dependent inflow properties with a co- operative dynamical system	17
2.1	Introduction . . . . .	17
2.2	The response of a model dynamical system to periodic perturbations	20
2.3	Conclusions . . . . .	34
2.4	Acknowledgement . . . . .	36
Chapter 3	Sensing time dependent inflow parameters with an enzymatic reaction	40
3.1	Introduction . . . . .	40
3.2	Determination of inflow properties with enzymatic reactions . . .	47
3.3	Conclusions . . . . .	65
3.4	Acknowledgement . . . . .	66
Chapter 4	Emergence of Many Mini-Circles from a Coffee Suspension with Mechanical Rotation	72
4.1	Introduction . . . . .	72
4.2	Materials and Methods . . . . .	73
4.3	Results and Discussion . . . . .	74

4.4	Conclusions . . . . .	81
Chapter 5	General Conclusion	89
5.1	Overview . . . . .	89
5.2	Open questions and Future problems . . . . .	89

# List of Figures

2.1	Positions of nullclines for the dynamical system defined by Eqs.(2.2,2.3). .....	24
2.2	Time evolution of the dynamical system described by Eqs.(2.2,2.3) as a function of the inflow frequency $f$ for a fixed amplitude $A = 0.12$ . .	25
2.3	Time evolution of the dynamical system described by Eqs.(2.2,2.3) as a function of the inflow amplitude $A$ for a fixed frequency $f = 0.05$ . .	26
2.4	Geometrical illustration of types of oscillation in the classification based on $y_{min}$ and $y_{max}$ . . . . .	29
2.5	Phase diagram showing the type of oscillation as a function of inflow parameters $(f, A)$ . . . . .	31
2.6	Phase diagram showing the type of oscillation as a function of inflow parameters $(f, A)$ . . . . .	32
2.7	Phase diagram showing the type of oscillation as a function of inflow parameters $(f, A)$ . . . . .	33
3.1	Positions of nullclines for the dynamical system defined by Eqs.(3.10,3.11) in the phase space $(x, y)$ . . . . .	52
3.2	The concentration of $Y$ as a function of time for the fixed amplitude $A = 1.2$ and a few different frequencies. . . . .	56
3.3	The phase diagram showing the oscillation type as a function of inflow parameters $(\nu, A)$ . . . . .	57

3.4	Positions of nullclines for the dynamical system defined by Eqs.(3.19,3.20) in the phase space $(x, y)$ . . . . .	61
3.5	The concentration of $Y$ as a function of time for the model in which the enzyme molecule is activated by three molecules of reagent. . . . .	63
3.6	The phase diagram showing the oscillation type a the function of inflow parameters $(\nu, A)$ . . . . .	64
4.1	Experimental scheme. (a) Roasted coffee beans were ground with a conical burr grinder. (b) Experimental apparatus to rotate the tilted dish with the solution containing the coffee particles. . . . .	75
4.2	Generation of various characteristic patterns from a drying solution containing coffee powder under different conditions. . . . .	76
4.3	Segregation pattern obtained from numerical simulation for phase-segregation with the simple model equations (Equations (1)–(3)). . . . .	80

# List of Tables

2.1	The classification of oscillations . . . . .	27
-----	--	----

# Chapter 1

## General Introduction

Moreover this investigation seems likely to make a substantial contribution to the whole body of truth, and particularly to the study of nature; for the soul is in a sense the principle of animal life. – Aristoteles[1, 2]

### 1.1 Introduction

#### 1.1.1 Perspectives

Rhythm is ubiquitous in nature. Living system, even a living cell, has daily activities while the Sun revolves. These diurnal cycles are considered to be supported by circadian rhythm. Living organisms have adapted to rotation of the Earth, whereby they can predict its changing of environments. Moreover there are annual changes by revolution of the Earth round the Sun. Several flowers such as cherry blossom bloom once a year in Spring, perceiving the gradual changing of environment, for example the length of day time, although it can be cloudy or rainy. Time events surrounding living matter are not only year-to-year or day-to-day but also more frequent or could be sudden or with fluctuations. What does enable living organism to perceive the essential information of time events? This dissertation will propose its possibilities.

What is the first life form on the Earth with rhythm? Cyanobacteria have been found in

the oldest known fossils in Western Australia, which are around 3.5 billion years old[3], whereas the Earth is estimated to be circa 4.5 billion years old[4–7].

Cyanobacteria are considered not only as the possible first photosynthetic organism but also as the oldest life form having circadian clock. Cyanobacteria such as *Synechococcus elongatus* PCC 7942 exhibit 24-h rhythms of gene expression that are controlled by an endogenous circadian clock that is mechanistically distinct from those described for diverse eukaryotes[8].

‘The lock-and-key theory’ is a commonly accepted model in cell biology that cells receive external information on cell membrane and then maintain the dynamic functions by networks of enzyme and substrate alike lock and key[9]. In differentiation of cell or cancelation, however, it has been revealed that cell responses are observed to be all-or-none, and activities of hundreds of genes are considered to be controlled ON/OFF like.

The theoretical approach to the entropy of non-equilibrium open systems is difficult because it is difficult to count the number of microscopic states when the system is moving or flowing. However, a typical example of a system that maintains spatio-temporal order not by its own autonomous nature but by interaction with the outside is the living organism on the earth, which lives in homeostasis under the time changes of day and night and seasons caused by the rotation and revolution of the earth. If it were not for the changes of day and night and the seasons, would we have the creatures we have today? How can we maintain ourselves as a non-equilibrium open system in a changing environment? Against the background of these questions, the following studies, which constitute this dissertation, set up specific problems for systems that are given a period from the outside, and tackled them by combining theory and experiment as a challenge to the problems described above. The following three chapters give an overview of these studies.

Spontaneous emergence of spatio-temporal order is a phenomenon specific to non-equilibrium open systems, i.e. systems that exchange energy and matter with the outside

world. Herein, Spontaneous refers not only to the autonomous production of an object without external forces but also to the process by which an object progresses naturally, i.e. to a more stable state, over time even under fluctuations[10–13] or periodic environmental changes.

### 1.1.2 Organisation of the thesis

The remainder of this dissertation is organised into a section hereof for backgrounds and four chapters as follows.

Chapter 2 presents the results of mathematical modelling and numerical simulations of the emergence of temporal order (rhythm) under periodic environmental changes and discrimination of its periodical parameters as ON/OFF switching.

Chapter 3 considers a few models of allosteric enzymatic reactions and discuss their applicability for sensing the frequency or the amplitude of the reagent inflow.

In Chapter 4, the spontaneous emergence of a spatio-temporal order (pattern) during the drying of a suspension on an inclined turntable is shown employing experiments and theoretical analysis.

Finally, chapter 5 concludes these chapters above and provides an outlook for the future.

## 1.2 Backgrounds

*What is Life?*, written by an Austrian-Irish physicist Ervin Schrödinger, said that “what an organism feeds upon is negative entropy”[14, 15]. Plants have their nutrition as the most potent supply of ‘negative entropy’ in the sunlight.

The notion of entropy  $S$  was introduced into science by Rudolf Clausius (1822–1888) in 1850–1865. The change of entropy can be written as:

$$dS = \frac{\delta Q}{T} \tag{1.1}$$

where  $\delta Q$  is the heat obtained by the system at the absolute temperature  $T$  in the quasi-equilibrium process. Entropy measures irreversible dissipation of energy per unit temperature.

Ludwig Boltzmann (1844–1906) first stated the possible relationship between thermodynamic entropy and the microscopic properties of matter in his kinetic theory of gases:

$$S = k_B \ln W \quad (1.2)$$

where  $k_B$  is Boltzmann’s constant, and  $W$  is the number of possible microstates corresponding to the macroscopic state of the system.

In an isolated system having no interaction with the environment, the entropy production in a body is always above zero (the second law of thermodynamics), and eventually equilibrium will be reached and no macroscopic spatio-temporal structure will emerge. In contrast, in order to maintain temporal and spatial order, energy must be taken in from the outside and entropy must be disposed of outwards. Let us quote [14], “New laws to be expected in the Organism”. Such a system was named a “dissipative structure” by the Nobel laureate in chemistry, Prigogine. This is also known as a nonequilibrium open system. Beyond Schödinger’s predictions for living organisms, examples of self-organisation in non-living systems have been reported since the middle of the twentieth century. In non-equilibrium open systems, spatio-temporal patterns are generated spontaneously because a uniformly stationary state is unstable. So far, linear non-equilibrium thermodynamics and statistical mechanics have been established for equilibrium and near-equilibrium systems, such as the free energy minimization principle and the extremal principles of entropy production rate (Lars Onsager[16, 17], Ilya Prigogine[18–20], Hans Ziegler[21] et al.). However, the “far-from-equilibrium system” has not yet been systematised, and researchers in various fields are actively working on this problem system by theoretical, experimental, and numerical simulations, and by using various phenomena as subjects.

## References

- <sup>1</sup>A. Jannone and E. Barbotin, *Aristote De l'âme*, 4th ed., Collection des universités de France Série grecque 171 (Belles Lettres, Paris, 2009), 97 pp.
- <sup>2</sup>Aristoteles, *On the Soul. Parva Naturalia. On Breath*, trans. by W. S. Hett, Reprinted, Vol. 8, The Loeb Classical Library 288 (Harvard Univ. Press [u.a.], Cambridge, Mass, 1st Jan. 1957), 527 pp.
- <sup>3</sup>J. W. Schopf and B. M. Packer, 'Early Archean (3.3-billion to 3.5-billion-year-old) microfossils from Warrawoona Group, Australia', *Science* **237**, 70–73 (1987).
- <sup>4</sup>U. G. Survey, *Geologic Time: Age of the Earth*, (1997) <https://pubs.usgs.gov/gip/geotime/age.html> (visited on 29/11/2019).
- <sup>5</sup>G. B. Dalrymple, 'The age of the Earth in the twentieth century: a problem (mostly) solved', Geological Society, London, Special Publications **190**, 205–221 (2001).
- <sup>6</sup>G. Manhes, C. J. Allègre, B. Dupré and B. Hamelin, 'Lead isotope study of basic-ultrabasic layered complexes: Speculations about the age of the earth and primitive mantle characteristics', *Earth and Planetary Science Letters* **47**, 370–382 (1980).
- <sup>7</sup>P. S. Braterman, *How Science Figured Out the Age of Earth*, Scientific American, (2013) <https://www.scientificamerican.com/article/how-science-figured-out-the-age-of-the-earth/> (visited on 29/11/2019).
- <sup>8</sup>J. Ditty, S. Williams and S. Golden, 'A Cyanobacterial Circadian Timing Mechanism', *Annual Review of Genetics* **37**, 513–543 (2003).
- <sup>9</sup>E. Fischer, 'Einfluss der Configuration auf die Wirkung der Enzyme. II', *Berichte der deutschen chemischen Gesellschaft* **27**, 3479–3483 (1894).
- <sup>10</sup>Y. Sumino, N. Magome, T. Hamada and K. Yoshikawa, 'Self-Running Droplet: Emergence of Regular Motion from Nonequilibrium Noise', *Physical Review Letters* **94**, 068301 (2005).

- <sup>11</sup>Y. Sumino and K. Yoshikawa, ‘Self-motion of an oil droplet: A simple physicochemical model of active Brownian motion’, *Chaos: An Interdisciplinary Journal of Non-linear Science* **18**, 026106 (2008).
- <sup>12</sup>T. Kurimura, M. Ichikawa, M. Takinoue and K. Yoshikawa, ‘Back-and-forth micro-motion of aqueous droplets in a dc electric field’, *Physical Review E* **88**, 042918 (2013).
- <sup>13</sup>T. Kurimura and M. Ichikawa, ‘Noise-supported actuator: Coherent resonance in the oscillations of a micrometer-sized object under a direct current-voltage’, *Applied Physics Letters* **108**, 144101 (2016).
- <sup>14</sup>E. Schrödinger, *What is Life?: With Mind and Matter and Autobiographical Sketches*, Canto (Cambridge University Press, Cambridge, 1992).
- <sup>15</sup>L. M. Martyushev, ‘Entropy and Entropy Production: Old Misconceptions and New Breakthroughs’, *Entropy* **15**, 10.3390/e15041152 (2013).
- <sup>16</sup>L. Onsager, ‘Reciprocal Relations in Irreversible Processes. I.’, *Physical Review* **37**, 405–426 (1931).
- <sup>17</sup>L. Onsager, ‘Reciprocal Relations in Irreversible Processes. II.’, *Physical Review* **38**, 2265–2279 (1931).
- <sup>18</sup>I. Prigogine and P. V. Rysselberghe, ‘Introduction to Thermodynamics of Irreversible Processes’, *Journal of The Electrochemical Society* **110**, 97C (1963).
- <sup>19</sup>I. Prigogine, *Introduction to thermodynamics of irreversible processes* (1st Jan. 1967).
- <sup>20</sup>I. Prigogine, ‘Time, Structure, and Fluctuations’, *Science* **201**, 777–785 (1978).
- <sup>21</sup>H. Ziegler, ‘Some extremum principles in irreversible thermodynamics, with application to continuum mechanics’, *Progress in Solid Mechanics*, Vol. 4, 93–193 (1963).

## Chapter 2

# Discrimination of time-dependent inflow properties with a cooperative dynamical system

### 2.1 Introduction

Bistability and hysteresis are commonly observed in physics, chemistry and biology [1–6]. Let us assume that a system has two stable states  $S_1$  and  $S_2$  and that an increase in the value of control parameter  $\lambda$  above the threshold  $\lambda_1$  triggers the transition from  $S_1$  to  $S_2$ , whereas the reverse transition from  $S_2$  to  $S_1$  occurs if the value of the control parameter drops below  $\lambda_2$ . Such a system can obviously be used as a discriminator of the control parameter value. For example, if the initial state is  $S_1$  and after some time we observe the system in  $S_2$ , then at some point the value of the control parameter necessarily exceeded  $\lambda_1$ . However, if only time-monotonic changes in the value of the control parameter are considered, then the system discrimination ability is reduced to just two values ;  $\lambda_1$  and  $\lambda_2$ .

In this paper we demonstrate the suitability of a dynamical system characterized by

sigmoidal kinetics for discrimination-oriented applications, under a new strategy of imposing a periodic perturbation or input on a cooperative system. It has been reported [7–9] that periodic perturbations can significantly change the time evolution of a non-linear system. As a discriminator prototype, we consider a two-variable system in which the inflow of one of the variables is a control parameter. Numerical simulations reveal a non-trivial property of such a system: a marginal change in the inflow parameters (amplitude or frequency) can switch the response of a cooperative system between different branches in the stage diagram. The frequency at which such switching occurs is a monotonic function of the inflow amplitude. Therefore, at a fixed amplitude of periodic inflow, the observation of a transition between different types of oscillatory evolution of the system provides information which allows us to discriminate the inflow frequency. The above discussion does not necessarily limit the range of frequencies that can be discriminated by the observation of transitions between different types of oscillations. Similarly, for a fixed frequency of periodic inflow, transitions between different types of system oscillations occur within a narrow range of amplitudes. The transition can be used to discriminate the inflow amplitude, but for the model considered here, the useful range of such discrimination is rather limited.

In numerical simulations, we consider simple system dynamics defined by a single sigmoidal term expressed by a rational function, which is typical for enzymatic reactions [10–14]. In such reactions the appearance of sigmoidal kinetic behavior is usually interpreted to be the result of the interaction of substrates with enzymes through positive cooperative binding. Modeling of cooperative binding leads to the Hill equation [10]:

$$\theta = \frac{[L]^n}{K_d + [L]^n} \quad (2.1)$$

where  $\theta$  is the fraction of ligand binding sites filled,  $[L]$  is the ligand concentration,  $K_d$  is the apparent dissociation constant derived from the mass action law, and  $n$  is the Hill coefficient which represents the degree of cooperativity. If  $n = 1$ , there is no cooperativity; for  $n > 1$ , the cooperativity is positive. Kinetics with sigmoidal behavior are not limited to enzymatic reactions. This also describes the response of various biological

systems to external stimuli, including the effect of drug delivery, which is an interesting topic in pharmacology. Among the many experimental studies that have reported sigmoidal behavior, the Hill coefficient  $n$  usually has a value between 2 and 4 [10–20]. Here we selected  $n = 3$  for the numerical simulations presented below.

The paper is organized as follows. In the next section, we consider a bistable model and study its time evolution as a function of the amplitude and frequency of periodic inflow. We demonstrate how the system can be used as a discriminator and discuss the sources of discrimination errors. In the final section we argue that the observed phenomenon is generic and discuss its potential applications.

## 2.2 The response of a model dynamical system to periodic perturbations

Let us consider a dynamical system of two variables  $(x(t), y(t))$  defined by a set of differential equations:

$$\frac{dx}{dt} = g(x, y, t) = -\alpha x + y + A \cdot (\sin(2\pi f t + \phi_0) + 1) \cdot \Theta(t) \quad (2.2)$$

$$\frac{dy}{dt} = h(x, y) = \frac{1}{\varepsilon} \cdot \left( \frac{x^3}{1 + x^3} - y \right) \quad (2.3)$$

In Eq.(2.2), the last term  $I(t) = A \cdot (\sin(2\pi f t + \phi_0) + 1) \cdot \Theta(t)$  describes a periodic inflow of  $x$  with frequency  $f$  and initial (for  $t = 0$ ) phase  $\phi_0$ .  $\Theta(t)$  is the Heaviside step function. We assume that there is no inflow for  $t < 0$ , and it is switched on at  $t = 0$ . If  $\phi_0 = 3 \cdot \pi/2$ , then  $I(t)$  is a continuous function. In this case,  $I(t = 0) = 0$ . It then increases and finally oscillates. For any other phase, the inflow term is not continuous at  $t = 0$ ; for example, if  $\phi_0 = \pi/2$  and then  $I(t = 0) = 2 \cdot A$ .  $I(t)$  then decreases and finally oscillates. The inflow term is always non-negative. For  $t > 0$  the time average of  $I(t)$  equals  $A$  and is independent of the frequency and the initial phase. If the inflow amplitude  $A = 0$ , then  $(x = 0, y = 0)$  is the only steady state of Eqs.(2.2,2.3) and is stable. In the following analysis, we assume that the stable state of the system without flow is the initial state for the simulated evolution.

Initially, let us consider the time evolution of the system for a constant inflow  $I(t) = A > 0$  for  $t \geq 0$  (thus,  $f = 0$  and  $\phi_0 = 0$ ). The characteristics of the time evolution depend on the amplitude of the inflow term and on the initial state. In this case, the nullcline  $g(x, y, t) = 0$  is the time-independent line with a definite slope determined by the value of  $\alpha$  and a shift which depends on the inflow amplitude  $A$ . Figure 2.1 shows the location of nullclines, calculated for  $\varepsilon = 1$ ,  $\alpha = 0.55$  and a few different values of the inflow. Let us assume that  $A_1$  and  $A_2$  are the amplitudes for which the BN  $g(x, y) = 0$  nullcline is tangential to the sigmoidal-shaped nullcline  $h(x, y) = 0$ . The stable stationary states of

the system can be located on two branches on the  $h(x, y) = 0$  nullcline. One contains all of the points of the  $h(x, y) = 0$  nullcline located between point  $(0, 0)$  and the tangency point  $(x_1, y_1)$ . We will call it the lower stable branch (LSB). The other is the upper stable branch (USB), and is formed by all of the points of the  $h(x, y) = 0$  nullcline located above  $(x_2, y_2)$ . The stationary states located on the nullcline between  $(x_1, y_1)$  and  $(x_2, y_2)$  are unstable. In the case when  $A < A_2$ , the only stationary state is located on the lower stable branch, so the system converges to the stable state  $y_\infty = \lim_{t \rightarrow \infty} y(t)$  such that  $y_\infty \leq y_1$  regardless of the initial state. Similarly, for  $A > A_1$ , the single BN stationary state is located on the upper stable branch, and for all initial states the system converges to the stable state  $y_\infty \geq y_2$ . For  $A_2 \leq A \leq A_1$ , the stationary state that is approached for  $t \rightarrow \infty$  depends on the initial state and on the partition of the phase space determined by the separatrices of the saddle point which is located on the middle branch of the  $h$  nullcline. This analysis also applies when the frequency of inflow oscillations is very high. In such a case, the flow oscillations are much faster than both the system dynamics and the system responds to the time-averaged value of the inflow  $A$ .

For sufficiently slow oscillations of the inflow ( $0 < f \ll 1$ ), the system can follow the slowly relocating stable state, the position of which varies according to the instantaneous value of the inflow. If the initial state of the system is  $(x(0) = 0, y(0) = 0)$  and  $2 \cdot A \leq A_1$ , then  $y(t) \leq y_1$  for all  $t$ . Therefore, the system state oscillates along the lower stable branch of the  $h(x, y) = 0$  nullcline with the period defined by the frequency of inflow oscillations. If  $2 \cdot A > A_1$ , then there are intervals of time within which the system has a single stationary state located on the upper stable branch. During a single oscillation cycle, there are moments of time  $t_1$  and  $t_2$  at which  $y(t_1) \leq y_1$  and  $y(t_2) \geq y_2$ , and thus oscillations that extend over both stable branches are expected.

For moderate values of  $f$ , the system dynamics are too slow to closely follow the changes in the inflow value. In such a case, oscillations around a stable state located in the lower stable branch that extend to the unstable branch, as well as oscillations around a stable state located in the upper stable branch that extend to the unstable branch, should

be observed. This is confirmed by numerical simulations.

The complexity of oscillations observed for a constant inflow amplitude  $A = 0.12$  (thus  $A > A_1/2$  but  $A < A_1$ ) as a function of flow frequency is illustrated in Fig. 2.2. As discussed above, for the selected amplitude and a low frequency of inflow oscillations, the system dynamics follow the time-dependent stationary state and oscillations of  $y(t)$  extend over both stable branches of the  $h(x, y) = 0$  nullcline. For intermediate frequencies, oscillations accumulate on the upper stable branch of the nullcline and the minimum value of  $y(t)$  increases with frequency. Then, at a certain frequency  $f_c$  ( for the selected amplitude of oscillations,  $f_c \approx 0.0312$  ), the oscillations switch from the upper to the lower stable branch of the  $h(x, y) = 0$  nullcline. The transition between oscillations located on different stable branches is quite pronounced and should be easily detected in experiments with a system exhibiting hysteresis. Therefore, it becomes apparent that a cooperative system can discriminate the frequency of a perturbation if its amplitude remains fixed. Numerical simulations have also demonstrated that the frequency of the transition between oscillations on the USB and LSB depends on the phase  $\phi_0$ . The right upper corner of Fig. 2.2 shows two types of oscillations that are observed for  $f = 0.031$ . If  $\phi_0 = 0$ , the system oscillates at the upper stable branch, but if  $\phi_0 = \frac{3\pi}{2}$ , oscillations around the lower stable branch are seen. Fortunately for the application of this approach to discrimination, the interval of frequencies within which phase-dependent evolution is observed is very narrow. For  $A = 0.12$ , it is  $[0.0306, 0.0312]$ . The width of this interval ( $\Delta f \sim 0.0006$ ) defines the precision in frequency discrimination.

The dynamical system considered here can also be used to discriminate the amplitude of an applied perturbation. Figure 2.3 shows the time evolution of  $y(t)$  for a few values of perturbation amplitude  $A$  and a fixed inflow frequency ( $f = 0.05$ ). As expected, for small amplitudes ( $A \leq 0.1122$ ) the oscillations of  $y(t)$  are limited to the LSB. For larger amplitudes ( $0.1122 < A < 0.1361$ ), the range of observed values of  $y(t)$  increases, but the oscillations are still anchored on the LSB. Finally, if  $0.13617 \leq A$ , the oscillations

move onto the USB. The transition between the different types of oscillation is quite pronounced and can be used to discriminate the value of amplitude. Here, similar to the cases illustrated in Fig. 2.2, we observe a narrow interval of amplitudes ( $\Delta A \sim 0.0001$ ) within which the type of oscillation depends on the initial phase.

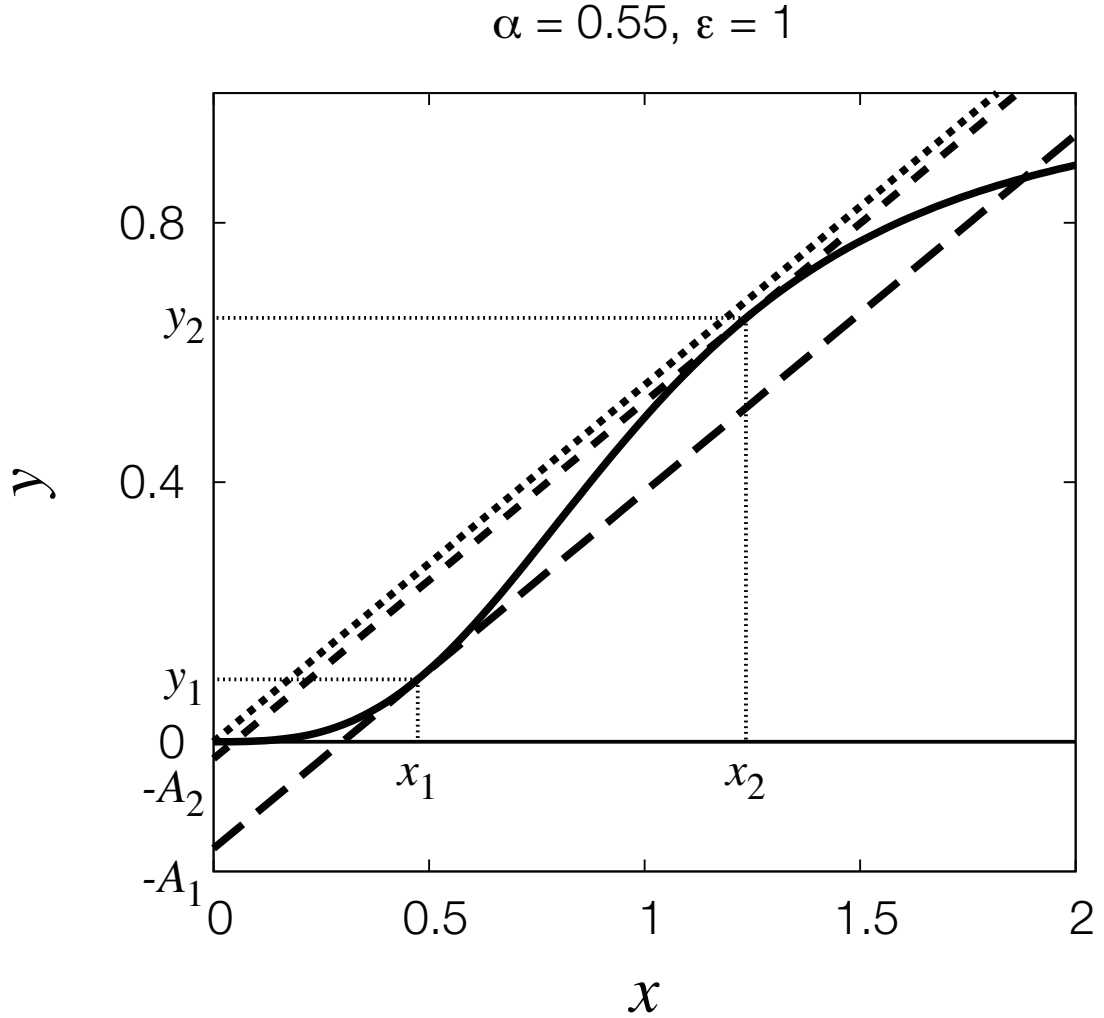


Figure2.1 Positions of nullclines for the dynamical system defined by Eqs.(2.2.2.3). The model parameters are:  $\varepsilon = 1$ ,  $\alpha = 0.55$ ,  $f = 0$  and  $\phi_0 = 0$ . The nullcline  $h(x, y) = 0$  is plotted with a solid line. The nullcline  $g(x, y, t) = 0$  is shown for a few cases:  $A = 0$  ( dotted line),  $A = A_2 = 0.02603$  ( short-dashed line),  $A = A_1 = 0.16445$  ( long-dashed line). For the selected parameters of the model, the variables at tangential points are  $(x_1, y_1) = (0.47368, 0.09607)$  and  $(x_2, y_2) = (1.23531, 0.65339)$ .

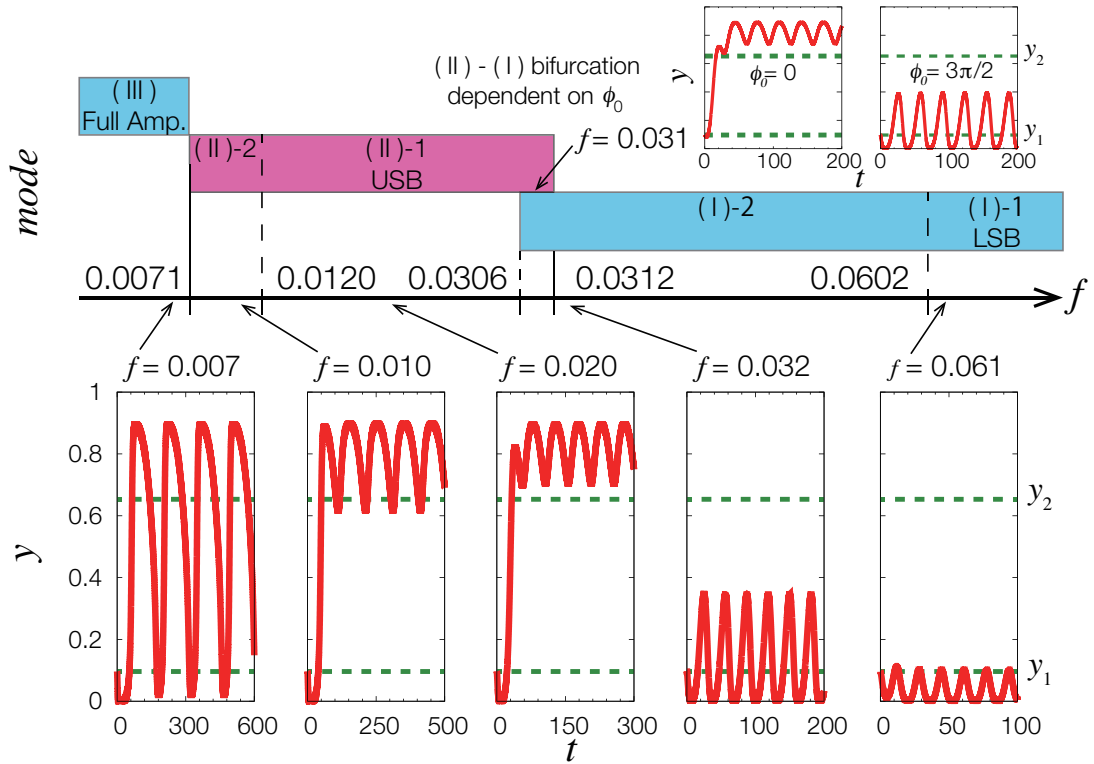


Figure 2.2 Time evolution of the dynamical system described by Eqs.(2.2,2.3) as a function of the inflow frequency  $f$  for a fixed amplitude  $A = 0.12$ . The model parameters are:  $\varepsilon = 1$ ,  $\alpha = 0.55$ . Tics and numbers on the frequency scale mark transitions between different types of oscillation. The initial phase is  $\phi_0 = 3\pi/2$  for all cases except on the left in the upper row, for which  $\phi_0 = 0$ . The horizontal dashed lines mark the values of  $y_1$  and  $y_2$ .

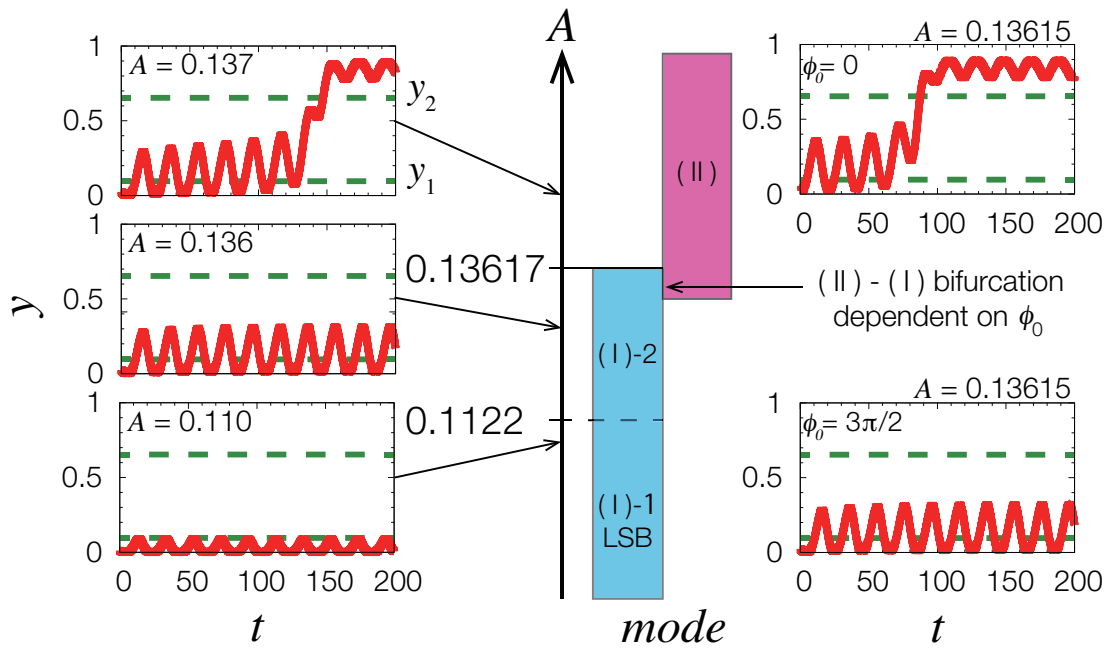


Figure 2.3 Time evolution of the dynamical system described by Eqs.(2.2,2.3) as a function of the inflow amplitude  $A$  for a fixed frequency  $f = 0.05$ . Tics and numbers on the frequency scale mark transitions between different types of oscillation. The initial phase is  $\phi_0 = 3\pi/2$  for all cases except at the top in the right column, for which  $\phi_0 = 0$ . The horizontal dashed lines mark the values of  $y_1$  and  $y_2$ .

To give a more precise description of system evolution, let us introduce a classification of oscillations based on the minimum and maximum values of  $y(t)$  observed over a long time interval for which the evolution has reached a stationary state. We define:

$$y_{min} = \min_{t \in [t_{min}, t_{max}]} y(t) \quad (2.4)$$

and

$$y_{max} = \max_{t \in [t_{min}, t_{max}]} y(t) \quad (2.5)$$

Initially, we used  $t_{min} = 1000$ , where  $t_{max} = t_{min} + 1000$ . Next we repeated the calculations for  $t_{min} = 2000$ . If there is a significant discrepancy in  $y_{min}, y_{max}$  obtained for these time intervals, then the procedure is repeated with  $t_{min}$  increased by an additional 1000 time units until agreement is attained.

The type of oscillation is classified through the comparison of  $y_{min}$  and  $y_{max}$  with the values of  $y_1$  and  $y_2$ , as illustrated in Fig. 2.4. The classification of oscillations is summarized in Table2.2.

Table2.1 The classification of oscillations

oscillation class	condition
(I)-1 LSB	$y_{min} \leq y_{max} < y_1$ (oscillations limited to LSB)
(I)-2	$y_{min} < y_1, y_1 \leq y_{max} < y_2$
(III)	$y_{min} < y_1, y_{max} \geq y_2$
(II)-2	$y_1 \leq y_{min} < y_2, y_{max} \geq y_2$
(II)-1 USB	$y_{max} \geq y_{min} > y_2$ (oscillations limited to USB)
(IV)	$y_1 \leq y_{min} < y_2, y_1 \leq y_{max} < y_2$

As shown in Fig. 2.4, the transitions between oscillation types  $(I) - 1LSB \leftrightarrow (I) - 2$

and  $(I) - 2 \leftrightarrow (III)$  are continuous because they result from an increase or decrease in the  $y_{max}$  value. Similarly, the transitions between oscillation types  $(III) \leftrightarrow (II) - 2$  and  $(II) - 2 \leftrightarrow (II) - 1USB$  are continuous because they are related to an increase or decrease in the  $y_{min}$  value. In actual experiments, these transitions are difficult to detect because they require highly accurate data acquisition. On the other hand, the transition  $(I) - 2 \leftrightarrow (II) - 1USB$ , on which the discrimination is based, can be easily detected because it is related to a discontinuous jump between  $y_{max} < y_2$  and  $y_{min} > y_2$ .

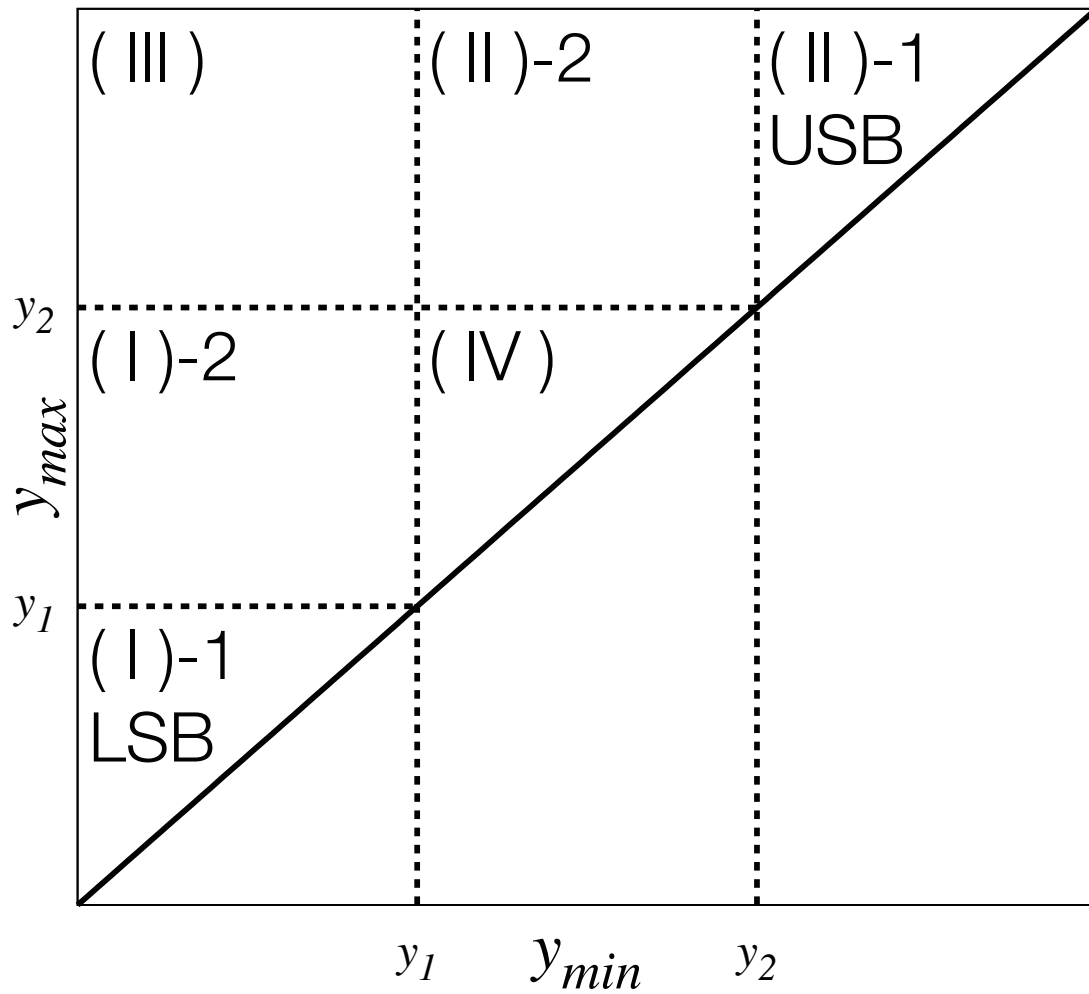


Figure2.4 Geometrical illustration of types of oscillation in the classification based on  $y_{min}$  and  $y_{max}$ . The dotted lines mark  $y_1 = 0.09607$  and  $y_2 = 0.65338$ .

Figure 2.5 illustrates the regions of parameters  $(f, A)$  for which a given oscillation pattern is observed in a model characterized by  $\alpha = 0.55$  and  $\varepsilon = 1$ . The thick line separates the region of the phase space  $(f, A)$  in which class (I)-2 oscillations are observed, from the region where class (II)-1 USB oscillations appear. Let us denote points on this line as  $(f_c, A_c)$ . The amplitude  $A_c$ , when treated as a function of  $f_c$ , is a continuous, monotonically increasing function  $A_c = G(f_c)$ . Therefore, the inverse function  $f_c = G^{-1}(A_c)$  exists. Our discrimination method is based on the determination of conditions in which a small change in  $f_c$  or  $A_c$  qualitatively changes the character of the time evolution to force a transition between (I) – 2 and (II) – 1 USB type oscillations. Let us assume that we want to measure the unknown inflow frequency and that we can regulate the inflow amplitude. The following procedure can be applied. Initially, we set a low amplitude so the system oscillates on the LSB (type (II) – 1 oscillations). Next, the amplitude is increased up to the moment  $A_z$  when oscillations of type (II) – 1 USB are detected. The frequency of inflow  $f_z$  can be estimated as  $f_z = G^{-1}(A_z)$ . This method works for all frequencies greater than  $f_0$ , which corresponds to the tip of the (II) – 1 USB region  $((f_0, A_0))$ . The accuracy of the estimation depends on the frequency and is high where the amplitude  $A_c$  is a rapidly increasing function of  $f_c$ , here for  $0.02 \leq f_c \leq 0.1$ . This system can also be used to determine the amplitude of inflow when we can control the frequency. Now we set a low frequency and the system exhibits type (III) oscillations. Next, the frequency is increased up to the moment  $f_y$  when oscillations of type (I) – 2 are detected. The amplitude of the inflow  $A_y$  is  $A_y = G(f_y)$ . Unlike for frequency, the range of discriminated amplitudes does not extend outside the interval  $[A_0, A_1]$ .

The phase diagrams, similar to that in Fig. 2.5 but for  $\varepsilon = 1/5$  and  $\varepsilon = 5$ , are shown in Fig. 2.6 and 2.7 respectively. The results are qualitatively identical to those in Fig. 2.5, suggesting that the described changes in the system oscillations are generic and should also apply to other systems with hysteresis influenced by a periodic perturbation.

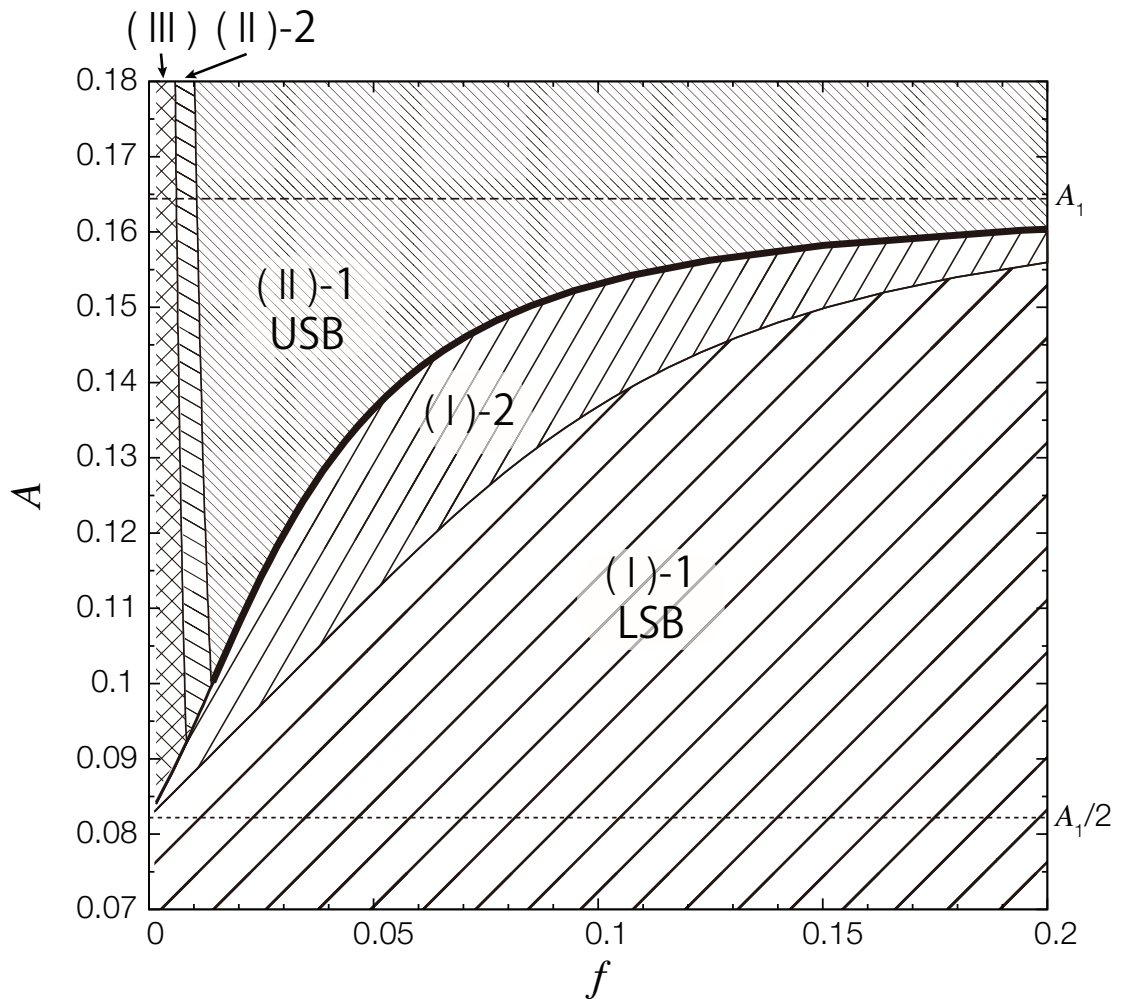


Figure 2.5 Phase diagram showing the type of oscillation as a function of inflow parameters  $(f, A)$ . The horizontal lines indicate  $A_1 = 0.16445$  and  $A_1/2$ . The model parameters are  $\varepsilon = 1$  and  $\alpha = 0.55$ . The thick solid line marks the boundary between oscillation classes  $(I) - 2$  and  $(II) - 1USB$ . The transition between these oscillations is used to determine the parameters of inflow.

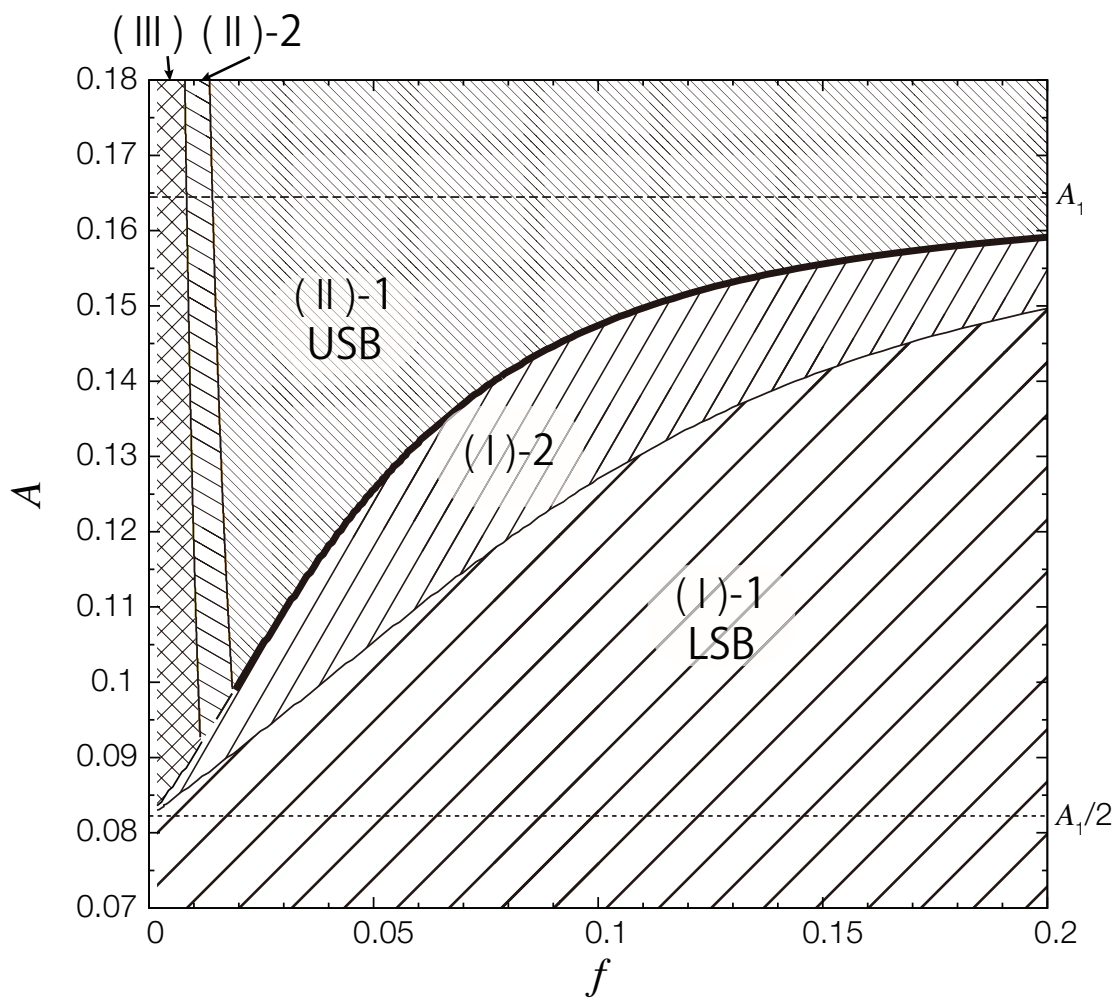


Figure 2.6 Phase diagram showing the type of oscillation as a function of inflow parameters  $(f, A)$ . The horizontal lines indicate  $A_1 = 0.16445$  and  $A_1/2$ . The model parameters are  $\varepsilon = 1/5$  and  $\alpha = 0.55$ .

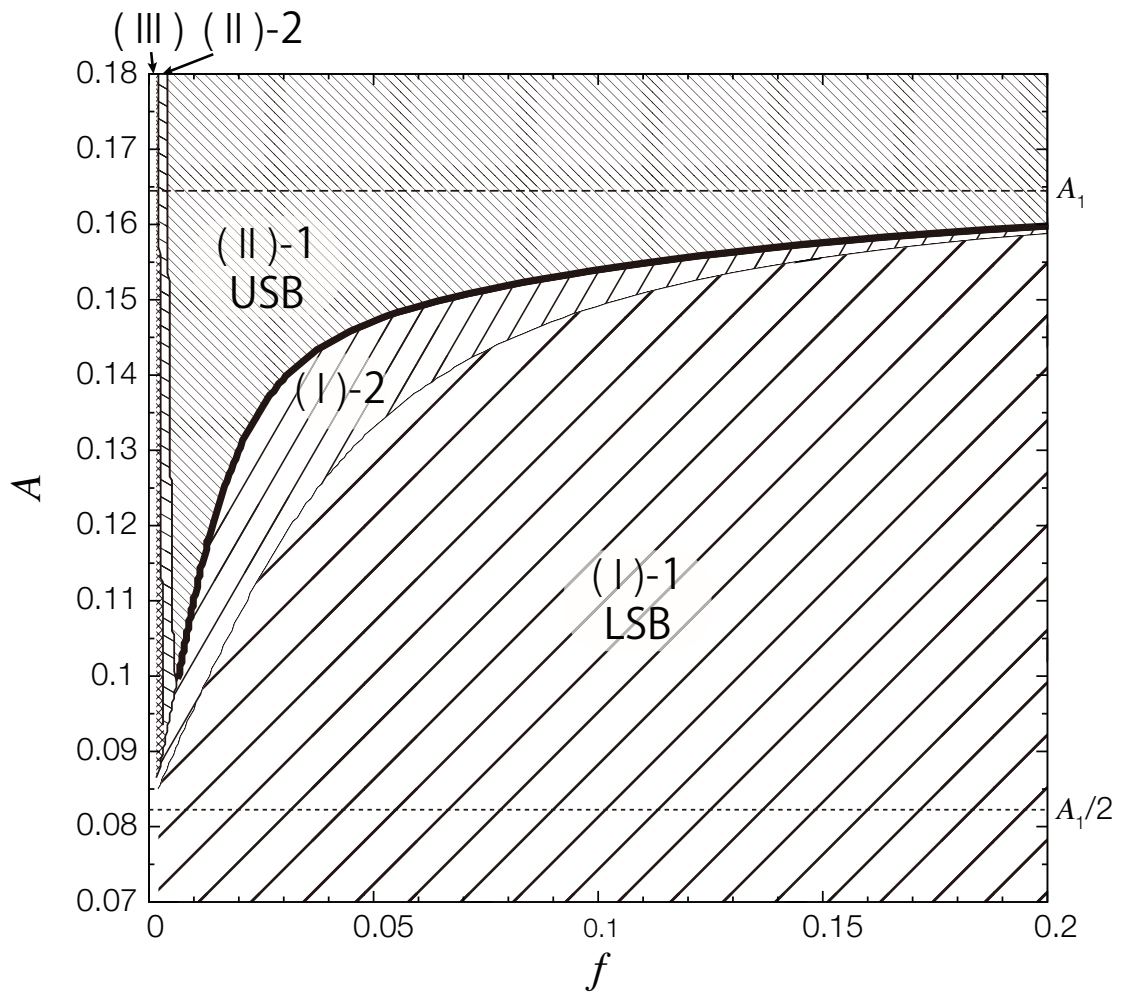


Figure2.7 Phase diagram showing the type of oscillation as a function of inflow parameters  $(f, A)$ . The horizontal lines indicate  $A_1 = 0.16445$  and  $A_1/2$ . The model parameters are  $\varepsilon = 5$  and  $\alpha = 0.55$ .

## 2.3 Conclusions

We have described how the time evolution of a cooperative system is dependent on the frequency and amplitude of a periodic stimulus. There is a narrow range of these parameters within which the characteristics of this evolution change in a qualitative manner: oscillations around one stable branch change into oscillations on another branch. This phenomenon can be used to determine the amplitude or frequency of an applied perturbation. As for the numerical framework, we evaluated the effect of the rhythmicity of substrate input in a model biochemical system with sigmoidal kinetics, i.e.  $n = 3$  in the Hill equation. Using numerical simulations, we separated the phase space of inflow parameters (amplitude and frequency) into regions where specific types of oscillation are observed. The boundary line separating oscillations with significantly different behaviors (type  $(I) - 2$  and type  $(II) - 1USB$  oscillations) was identified. The frequency that causes a transition appears in a monotonic function of the inflow amplitude. The system can be used to determine the inflow frequency if we can control the inflow amplitude. It can also be used to determine the inflow amplitude when we can control the frequency. In other words, sigmoidal kinetics with the Hill equation can act as an inflow discriminator.

This paper describes a system in which the nonlinear term in the kinetic equation for the  $y(t)$  variable is described by  $\frac{x^3}{1+x^3}$  term (cf. Eq.(2.3)) and the periodic inflow is described by a trigonometric function. We believe that these results are general, and qualitatively similar behavior can be expected in other systems with cooperative characteristics. We performed numerical simulations for a model based on Eqs.( 2.2,2.3) but with the inflow term in the form  $J(t) = A \cdot (\tanh(\gamma \cdot \sin(2\pi ft + \phi_0)) + 1) \cdot \Theta(t)$  for different values of  $\gamma$ . Such periodic inflow becomes a square-like wave for large  $\gamma$ . The phase diagrams that illustrate the type of oscillation as a function of  $f$  and  $A$  are qualitatively the same, as presented in Figs. ???. We also considered other nonlinear terms in the kinetic equation for  $y(t)$ , like  $\tanh(x - x_0)$  or  $1/(1 + \exp(-\delta \cdot (x - x_0)))$ , and

obtained similar results. Therefore, we believe that real systems of chemical reactions with hysteresis can be used as discriminators in the manner described above.

The present results can be regarded as a solution to the problem of the optimum stabilization of a system in an unstable state. Let us assume that Eqs.( 2.2,2.3) describe the time-dependent progress of a medical treatment where the variable  $y(t)$  represents the condition of a patient. The variable  $x(t)$  describes the time-dependent concentration of the curing drug. The states on the LSB and USB correspond to an ill and healthy patient, respectively. This simple model seems to realistically describe the basic features of drug therapy. It predicts that if the inflow of the drug is small, then the patient remains ill. Only a dose higher than a critical dose allows for successful treatment. However, some drugs are toxic ( such as those used in chemotherapy) and the total dose should be as small as possible. An analysis of the dynamical system presented in Fig. 2.5 can provide a solution: if we consider the periodic inflow of a drug in the form of Eq.(1), then the minimum amount of drug required to stabilize the patient in a healthy state corresponds to the bottom corner of the type  $(II) - 1USB$  oscillation region - here  $A_0 \cong 0.1$  and  $f_0 \cong 0.015$ .

Our results are expected to be applicable not only to natural sciences but also to social sciences too. Let us imagine a country with the two-party system in which the party N is naturally favored by the voters, and the result of party Y (the  $y$  variable) depends on its image generated by media (the  $x$  variable). The model based on Eqs.(2.2, 2.3) reflects realistic behavior of society. Equation (2.3) says that the support for party Y decreases in time because people prefer the party N and that irrespectively on high media pressure it saturates at a flat level. Equation (2.2) describes the decline of propaganda effect in time ( $-\alpha x$  term) and the influence of news (the inflow term). It also says that the support for party Y increases its media image. Our analysis indicates that the success of party Y (  $(II) - 1USB$  oscillations ) can be achieved with the minimum effort if the propaganda is periodically applied.

The properties of considered system represented by a thick solid line on Figs. ??

can be also interpreted within the binary logic. For a fixed inflow frequency  $f$  we can say, that  $(II) - 1USB$  class oscillations represent the logic (TRUE) state and the oscillations of (I) classes correspond to the logic 0 (FALSE). Now the amplitude discriminator described in the paper can be regarded as the simplest analog (amplitude) to 1-bit digital converter with the threshold amplitude  $G(f)$ . If just two values of amplitude ( $A_T, A_F$ ;  $A_F < G(f) < A_T$ ) are considered then the system operates as the identity gate or as a negation gate depending on which logic states are associated with these values. More complex logic functions can be also executed by the medium if the inflow term is a function of a few parameters, for example, in the form  $I(t) = (A_a \cdot (\sin(2\pi f_a t + \phi_0) + 1) + A_b \cdot (\sin(2\pi f_b t + \phi_0) + 1)) \cdot \Theta(t)$ . Following the idea of Ref. [21] the implementation of basic logic gate can be introduced in the considered system.

## 2.4 Acknowledgement

This work was supported by KAKENHI Grants-in-Aid for Scientific Research (15H02121, 25103012).

## References

- <sup>1</sup>J. D. Murray, *Mathematical biology*, 3rd ed, Vol. 17, Interdisciplinary Applied Mathematics (Springer, New York, 2002), 2 pp.
- <sup>2</sup>М. А. Красносельский and А. В. Покровский, *Системы с гистерезисом* (Наука, 1983).
- <sup>3</sup>М. А. Krasnosel'skii and А. V. Pokrovskii, *Systems with Hysteresis* (Springer-Verlag, Berlin Heidelberg, 1989).
- <sup>4</sup>K. Yoshikawa and N. Yoshinaga, 'Novel scenario of the folding transition of a single chain', *Journal of Physics: Condensed Matter* **17**, S2817–S2823 (2005).
- <sup>5</sup>M. I. Stefan and N. Le Novère, 'Cooperative Binding', *PLoS Computational Biology* **9**, edited by S. Wodak, e1003106 (2013).
- <sup>6</sup>K. Tsumoto, F. Luckel and K. Yoshikawa, 'Giant DNA molecules exhibit on/off switching of transcriptional activity through conformational transition', *Biophysical Chemistry* **106**, 23–29 (2003).
- <sup>7</sup>A. L. Kawczyński, 'Nonlinear resonances, quasiperiodicity and chaos in a periodically perturbed oscillatory chemical system with infinite number of bifurcations', *Polish Journal of Chemistry* **69**, 296–307 (1995).
- <sup>8</sup>A. L. Kawczyński and K. Bar-Eli, 'Periodic Perturbations and Three-Branch Return Maps of an Oscillatory Chemical System', *The Journal of Physical Chemistry* **99**, 16636–16640 (1995).
- <sup>9</sup>A. L. Kawczyński, 'Periodic perturbations of chaotic dynamics induce order', *Polish Journal of Chemistry* **70**, 643–655 (1996).
- <sup>10</sup>A. V. Hill, 'The possible effects of the aggregation of the molecules of haemoglobin on its dissociation curves', in *Proceedings of the Physiological Society* (22nd Jan. 1910), pp. iv–vii.

- <sup>11</sup>S. Goutelle, M. Maurin, F. Rougier, X. Barbaut, L. Bourguignon, M. Ducher and P. Maire, ‘The Hill equation: a review of its capabilities in pharmacological modelling’, *Fundamental & Clinical Pharmacology* **22**, 633–648 (2008).
- <sup>12</sup>J. Keener and J. Sneryd, *Mathematical Physiology I: Cellular Physiology, II: Systems Physiology*, 2nd ed., Vol. 8/2, Interdisciplinary Applied Mathematics (Springer-Verlag New York, 2009), XV, 549.
- <sup>13</sup>J. J. Tyson, ‘Biochemical Oscillations’, in *Computational Cell Biology*, edited by C. P. Fall, E. S. Marland, J. M. Wagner and J. J. Tyson (Springer New York, New York, NY, 2002), pp. 230–260.
- <sup>14</sup>R. Heinrich, S. Rapoport and T. Rapoport, ‘Metabolic regulation and mathematical models’, *Progress in Biophysics and Molecular Biology* **32**, 1–82 (1978).
- <sup>15</sup>J. Vera, O. Rath, E. Balsa-Canto, J. R. Banga, W. Kolch and O. Wolkenhauer, ‘Investigating dynamics of inhibitory and feedback loops in ERK signalling using power-law models’, *Molecular BioSystems* **6**, 2174–2191 (2010).
- <sup>16</sup>R. Blossey, J.-F. Bodart, A. Devys, T. Goudon and P. Lafitte, ‘Signal propagation of the MAPK cascade in *Xenopus* oocytes: role of bistability and ultrasensitivity for a mixed problem’, *Journal of Mathematical Biology* **64**, 1–39 (2012).
- <sup>17</sup>L. Qiao, R. B. Nachbar, I. G. Kevrekidis and S. Y. Shvartsman, ‘Bistability and Oscillations in the Huang-Ferrell Model of MAPK Signaling’, *PLOS Computational Biology* **3**, e184 (2007).
- <sup>18</sup>M. Zumsande and T. Gross, ‘Bifurcations and chaos in the MAPK signaling cascade’, *Journal of Theoretical Biology* **265**, 481–491 (2010).
- <sup>19</sup>T. Tsuruyama, T. Nakamura, G. Jin, M. Ozeki, Y. Yamada and H. Hiai, ‘Constitutive activation of Stat5a by retrovirus integration in early pre-B lymphomas of SL/Kh strain mice’, *Proceedings of the National Academy of Sciences* **99**, 8253–8258 (2002).
- <sup>20</sup>T. Tsuruyama, ‘A Model of Cell Biological Signaling Predicts a Phase Transition of Signaling and Provides Mathematical Formulae’, *PLOS ONE* **9**, e102911 (2014).

<sup>21</sup>J. Borresen and S. Lynch, 'Oscillatory Threshold Logic', PLOS ONE 7, e48498 (2012).

## Chapter 3

# Sensing time dependent inflow parameters with an enzymatic reaction

### 3.1 Introduction

The field of unconventional computation is concerned with investigation of computing media as alternatives to the standard semiconductor based electronics. The progress of silicon microprocessor technology, measured by the Moore law, is unprecedented in the history of civilization. However, it is anticipated that this trend should finally terminate. New computational strategies, new types of computing substrates and methods of information coding are needed to ensure the present rate of progress in construction of information processing devices[1–6].

Studies on information processing based on chemical reactions bring a significant contribution to unconventional computations. Some of chemical processes considered for information processing operations involve a few molecules only [7, 8]. This observation is promising because it shows that the future computing devices, based on chemical

reactions, can be reduced to the molecular scale.

Many chemical processes with potential applications to computationally oriented tasks can be found in Nature. Among them there are reactions leading to spatial structures formed by replicable molecules like RNA or DNA[9–12] and enzymatic processes characterized by complex, nonlinear chemical kinetics and exhibiting a rich variety of stationary spatio-temporal structures. Studies aimed on integration of these both approaches, for example: an interface that enables communication of otherwise incompatible nucleic-acid and enzyme computational systems, has been recently reported [13].

The enzymatic systems, we are concerned with accept and transform information in the form of chemical substrates with particular properties that meet the binding specificity criteria of a selected enzyme in a lock and key fashion. Enzymatic reactions can process information, coded in concentrations of specific molecules, catalyzing reactions and producing reaction products with different properties than the input reagents. The output information is coded in concentrations of products. The products can then participate in further chemical reactions. The transformations of products into yet other molecules can be regarded as following information processing steps. Studies on networks of connected enzyme-catalyzed reactions, with added chemical and enzymatic processes that incorporate the filtering steps into the functioning of this biocatalytic cascades have been recently published ( see [14]). It has been demonstrated that scaled logic variables for the inputs, output, and some intermediate products can be useful in describing enzyme cascade behavior by identifying quantities that offer the most direct control of the network properties. Therefore, using enzymatic reactions we can design information processing cascades, feedback loops, and other complex sequences of operations.

Studies on applications of chemical computing have a long history. It has been noticed that within the Michaelis–Menten kinetics model the shape of the convex line representing the rate of product production as the function of substrate concentration is similar to the relationship between the collector-emitter voltage and collector current in a bipolar

transistor. Using this analogy the concepts of transistor based information processing devices can be re-formulated in the language of chemical reactions and reagent flows. The theoretical background to chemistry based logic was presented in a number of publications Hjelmfelt and Ross and their co-workers [15–18]. They considered a perfectly stirred system and assumed that binary information is coded in stationary concentrations of reagents involved. In the proposed models of chemical neurons the stationary output concentration rapidly switches from low to high values if the concentration of the input reagent exceeds a specific value. In such case the relationship between reagent concentrations and binary logic values is straightforward, high concentrations represent the logic TRUE state, the low ones are interpreted as the logic FALSE. Simulation studies demonstrated how to implement the basic logic operations within the model of a chemical neuron [18, 19].

A convex line representing the relationship between the substrate concentration and the rate of product generation is typical for enzymatic reactions. For such relationship there is an identifiable linear regime, typically near the physical zero concentrations, as well as the saturation regime for larger concentrations. Most experimental studies on (bio)chemical information processing have been focused on the binary logic [20]. Low and high concentrations of selected reagents are interpreted as the logic variables. In this respect, a sigmoid, filter-like relationship between the substrate concentration and the product generation rate seems to be more suited for information processing applications, because it gives a better balance between low and high values of concentrations. Moreover, for information coded in stationary values of concentrations the sigmoidal response has advantage over the convex one because it allows to reduce noise of the output element important for noise-tolerant networking for chemical information processing [21].

It has been observed that sigmoidal kinetics can appear for properly chained enzymatic reactions [22]. Therefore such kinetics can be designed on demand by coupling an enzymatic process characterized by a convex kinetics with other reactions [23]. Different

physical or chemical stimuli can be applied to impact enzymatic processes. For example it was demonstrated that in enzymatic reaction involving glucose oxidase system response depends on initial concentration of hexokinase and ATP [23]. Even more interesting it has been observed that the transition between convex and sigmoidal kinetics can be achieved by system illumination [24].

The sigmoidal kinetics can be also expected for allosteric enzymatic reactions[25–27]. Allosteric regulation is one of many ways in which enzyme activity can be controlled. Enzyme activity is regulated by its conformational dynamics [28]. A typical enzyme contains binding sites where substrate molecules can be attached and the catalytic site where the activation energy is reduced and the reaction, specific for a given enzyme, proceeds. The allosteric enzymes contain another region, separated from the substrate binding site, to which small, regulatory molecules can attach to and thereby control the catalytic activity. The allosteric regulatory molecules change the conformation or dynamics of the enzyme that is transduced to the active site and thus affect the reaction rate of the enzyme. In this way, allosteric interactions can either inhibit or activate enzymes. As we demonstrate below, the regulating reactions can couple with the main enzymatic process. If the rates for these processes are properly selected then the resulting kinetics of an enzymatic reaction has a sigmoidal form.

The recent studies on applications of enzymatic reactions for computing oriented tasks match experiments with numerical simulations. It has been demonstrated that the simple information processing devices can be constructed with properly selected enzymatic reactions. Biocatalytic system with a double-sigmoid filter (sigmoid with respect to two types of molecules) are especially interesting because they can directly operate on two input signals [28–30]. Enzymatic reactions capable of recognizing two specific molecules or ions in the solution (for example  $Mg_2^+$  and  $Ca_2^+$  [28, 31]) were identified and their applications for construction of the logic gates (the AND binary gate [32], the OR binary gate [33]) have been reported. Enzymatic systems capable of more complex computational tasks like three-input logic gates or molecular full adders were also

reported [34, 35].

The studies discussed above were based on information coded in time-independent, stationary concentrations of selected reagents. Here we present a new approach to chemical sensing based on enzymatic reaction with information coded in time dependent evolution of the medium. We discuss an application of chemical computing to time dependent phenomena considering the problem of discrimination of the parameters describing periodic perturbations of a computing medium.

Living organisms have to process information in order to find the optimum environment for their existence under time-dependent environmental change. A significant part of their computational activity is focused on decision making. In a highly organized society life of its members is determined by the choices they make. Some of decision making problems require a binary (YES or NO) answer. Having in mind that information processing activity of living organisms is based on (bio-)chemical reactions we search for and identify chemical reaction models that can be applied for decision making problems in which the input information is coded in periodically changing inflow of reagents. Such inflow can be related to a periodic stimulus forced by cycling change in environment, like the circadian rhythm.

Rational decision making is based on time-dependent information about the problem. Information can be collected by chemical reactions showing different behaviour depending on the conditions they proceed in. A number of information processing strategies, operating on time dependent inputs have been reported in the literature [1–4]. An answer coming from a chemical sensor can be continuous or discrete. For example, one can get information on the distance to a source of excitations by comparing the frequency of pulses excited in a few identical excitable channels [36, 37]. An excitable chemical medium can be also applied as a sensor of critical changes in time dependent medium parameters. It has been demonstrated [38] that an excitation pulse can propagate in the medium with a slowly decreasing excitability level. On the other hand if exactly the same decrease in system excitability occurs rapidly then the excitation pulse van-

ishes. Therefore, by observing a distance propagated by a pulse in an excitable medium we are able to determine the rate of temporal changes in the medium excitability. The simplest sensors are binary discriminators (or binary classifiers). They are capable of distinguishing if the conditions at which reactions proceed belong to a given class or not. For example, an excitable medium with a propagating pulse can be regarded as a discriminator if the temporal changes in its excitability are larger than a given value.

The examples presented above illustrate sensing potential of a spatially distributed medium. However, there are reactions that proceed in a homogeneous medium that can be used as discriminators of the conditions in which it proceeds. In the previous chapter [39] we considered a dynamical system with hysteresis as a prototype of a decision making automaton. Systems with hysteresis, commonly observed in physics, chemistry and biology [40–42], are natural candidates for binary classifiers. In a system with hysteresis one can distinguish two different classes of stable states  $S_1$  and  $S_2$ . System evolution towards a state from a particular class is determined by the value of control parameter  $\lambda$  and the initial condition. Let us assume that the increase in control parameter  $\lambda$  value above the threshold  $\lambda_1$  triggers the transition from  $S_1$  to  $S_2$ . The reverse transition from  $S_2$  to  $S_1$  occurs if the value of control parameter drops below  $\lambda_2$ . Such a system can be obviously used as a discriminator of the control parameter. For example, if the initial state belongs to  $S_1$  and if after some time we observe the system in a state belonging to  $S_2$  then it means that at a certain moment of time the value of control parameter necessarily exceeded  $\lambda_1$ . However, if only time monotonic changes in the value of control parameter are considered then the system discrimination ability is reduced to just two values  $\lambda_1$  and  $\lambda_2$ .

We have recently demonstrated [39] that the applicability of a dynamical system characterized by sigmoidal kinetics for discrimination oriented tasks increases if a periodic perturbation of inflow is imposed. Periodically perturbed bistable system oscillates. The location of system oscillations in the phase space and the oscillation amplitude depend on the amplitude and frequency of perturbation. In particular we can distinguish os-

cillations between states in the class  $S_1$  and oscillations between states in the class  $S_2$ . The numerical simulations for reaction kinetics defined by a third order rational function revealed a non-trivial property of such system: a marginal change of inflow parameters (amplitude or frequency) can force a sharp transition between oscillations belonging to different classes. The transition occurs in a narrow range of perturbation parameters. The change between oscillation types can be easily distinguished and therefore a chemical reaction exhibiting hysteresis can be used as a discriminator of perturbation properties.

In this report we concentrate on realistic models of enzymatic reactions that can be applied as discriminators of periodically changing stimuli. All models are analyzed assuming that the reaction kinetics follows the mass action law. We consider model enzymatic reactions in which an enzyme is activated by one, two or three identical control molecules. The applicability of such models as sensors of inflow parameters is investigated. We start with the simplest reaction model in which an enzyme is activated by binding with a single molecule and demonstrate that such reaction model does not work as a discriminator of inflow. However, enzymatic reactions involving allosteric activation by two or three control molecules lead to a medium exhibiting bistability if the reaction rates are properly selected. These models lead to kinetic term in a Hill-like form with the Hill coefficient equal to 2 and 3, which value is typical for allosteric reactions characterized by a positive cooperativity [26, 43]. For both reaction models there is a sharp transition in the character of oscillations in product concentration in the phase space of parameters describing amplitude and frequency of periodic inflow of control molecules. Therefore, these enzymatic reactions can be used as binary discriminators of the periodic inflow parameters.

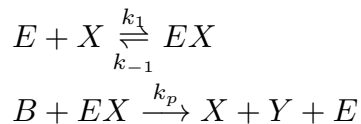
For sigmoidal kinetic we are able to stabilize oscillations in different regions of the phase space and we observe a sharp transition between oscillations of different classes. As discussed in this chapter such effect is absent for the case of convex kinetics.

## 3.2 Determination of inflow properties with enzymatic reactions

In this Section we consider three models of an enzymatic reaction and estimate their applicability for sensing oriented applications. In all models the enzyme  $E$  has to bind with a number of control molecules  $X$  to perform its function. The complex of enzyme and  $X$  transforms the reactant  $B$  into the product  $Y$ . We assume that the complex disintegrates after the reaction and all molecules of  $X$  are detached at the same time.

### 3.2.1 Enzyme activation with a single control molecule

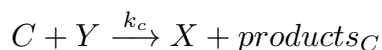
At the beginning we consider a model in which a single molecule of  $X$  activates the enzyme:



It is easy to notice that the sum of concentration of  $E$  ( $e$ ) and of  $EX$  ( $f$ ) does not change in time.

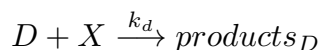
In all models discussed in this Section we assume that reagents  $X$  and  $Y$  are involved in the following processes:

transformation of product  $Y$  into reactant  $X$ :



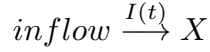
and

the decomposition of reactant  $X$ :



We assume that  $products_C$  and  $products_D$  are inert for all reactions listed above, so there is no need to specify them. The last of listed reactions removes  $X$  from the system, so the concentration of  $X$  ( $x$ ) tends to zero at long times. In order to have other, more

interesting behaviour of the system we assume that there is a time dependent inflow of the reagent  $X$  to the system described by a time dependent function  $I(t)$ :



For the following analysis we assume that concentrations of reagents  $B, C$  and  $D$  (denoted as  $b, c$  and  $d$ , respectively) are much larger than of the other reagents and we can assume that they remain constant in time. Therefore, the complete description of the system is given by three kinetic equations describing the time evolution of the concentrations of  $EX$  ( $f(t)$ ),  $X$  ( $x(t)$ ) and  $Y$  ( $y(t)$ ) read:

$$\frac{dx(t)}{dt} = -k_1ex(t) + k_{-1}f(t) + k_pbf(t) - k_dx(t) + k_cy(t) + I(t) \quad (3.1)$$

$$\frac{df(t)}{dt} = k_1ex(t) - k_{-1}f(t) - k_pbf(t) \quad (3.2)$$

$$\frac{dy(t)}{dt} = k_pbf(t) - k_cy(t) \quad (3.3)$$

If we assume that the reactions involving enzyme and its complex are fast, and those leading to *products<sub>C</sub>* and *products<sub>D</sub>* are slow then the concentration of  $EX$  complex can be regarded as quasistationary one. In such case the system time evolution description reduces to two kinetic equations for  $x(t)$  and  $y(t)$ :

$$\frac{dx(t)}{dt} = -k_dx(t) + k_cy(t) + I(t) \quad (3.4)$$

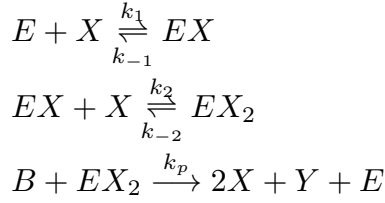
$$\frac{dy(t)}{dt} = \frac{k_1k_pb e_0 x(t)}{k_{-1} + k_pb + k_1x(t)} - k_cy(t) \quad (3.5)$$

Here the symbol  $e_0$  denotes the total concentration of enzyme in its free  $E$  and complexed forms  $EX$  ( $e_0 = e(t) + f(t) = \text{const.}$ ).

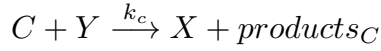
If the inflow is constant  $I(t) = A_0$  then the analysis of nullclines for the dynamical system (4-5) shows that for each set of model parameters (rate constants and concentrations of reagents that do not change in time) the system has a single, stable, stationary state. Therefore, the enzymatic reaction with activation by a single control molecule does not function as a discriminator of time dependent inflow parameters according to the strategy described in [39].

### 3.2.2 Enzyme activation with two control molecules

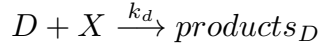
Hysteresis is observed in a slightly more complex reaction model in which the enzyme molecule  $E$  has to combine with two molecules of reagent  $X$  in order to transform the reactant  $B$  into the final product  $Y$ :



As in the previous model we consider the transformation of product  $Y$  into reactant  $X$ :



and the decomposition of reactant  $X$ :



The complete description of such reaction model is given by four kinetic equations describing the time evolution of  $f(t)$ ,  $x(t)$ ,  $y(t)$  and the concentrations of  $EX_2$  ( $g(t)$ ):

$$\frac{dx(t)}{dt} = -k_1e(t)x(t) + k_{-1}f(t) - k_2f(t)x(t) + k_{-2}g(t) + 2k_pbg(t) - k_dx(t) + k_ccy(t) + I(t) \quad (3.6)$$

$$\frac{df(t)}{dt} = k_1e(t)x(t) - k_{-1}f(t) - k_2f(t)x(t) + k_{-2}g(t) \quad (3.7)$$

$$\frac{dg(t)}{dt} = k_2f(t)x(t) - k_{-2}g(t) - k_pbg(t) \quad (3.8)$$

$$\frac{dy(t)}{dt} = k_pbg(t) - k_ccy(t) \quad (3.9)$$

If we assume that the reactions involving enzyme and its complexes are faster than those leading to *products<sub>C</sub>* and *products<sub>D</sub>* then the concentrations of complexes *EX* and *EX<sub>2</sub>* can be regarded as quasistationary ones. In such case the time evolution of the system is described by two kinetic equations for  $x(t)$  and  $y(t)$ :

$$\begin{aligned}\frac{dx(t)}{dt} &= Q(x(t), y(t), t) \\ &= -k_d dx(t) + k_c cy(t) + I(t)\end{aligned}\quad (3.10)$$

$$\begin{aligned}\frac{dy(t)}{dt} &= R(x(t), y(t)) \\ &= \frac{k_1 k_2 k_p b e_0 x^2(t)}{k_{-1} k_{-2} + k_1 k_p b + k_1 k_{-2} x(t) + k_1 k_p b x(t) + k_2 k_p b x(t) + k_1 k_2 x^2(t) - k_c c y(t)}\end{aligned}\quad (3.11)$$

where  $e_0$  denotes the total concentration of enzyme in its free and all complexed forms ( $e_0 = e(t) + f(t) + g(t) = \text{const.}$ ).

For this reaction model one can select the values of parameters such that the nullcline of Eq.(11) has a sigmoidal form, so the system exhibits hysteresis. For example, such behaviour is observed when  $b = c = d = e_0 = 1$ , the rate constants for fast reactions are  $k_1 = 10, k_{-1} = 200, k_2 = 20, k_{-2} = 160, k_p = 40$  and the rate constants for the slow reactions leading to products are  $k_c = 0.1, k_d = 1$ . Figure 1 illustrates the nullclines for these values of parameters. The nullcline  $Q(x, y, t) = 0$  is shown for a few values of inflow:  $I(t) \equiv 0$  (no inflow of  $X$ ),  $I(t) \equiv 0.731284$  and  $I(t) \equiv 1.64789 = A_1$ . The last two values of inflow correspond to cases when the nullcline  $Q(x, y, t)$  is tangential to the nullcline  $R(x, y)$ . At the beginning we consider an inflow that remains constant after it is switched on at  $t = 0$ , ie.:  $I(t) = I_0 \cdot \Theta(t)$ , where  $\Theta(t)$  is the Heaviside step function. If the inflow  $I_0 < 0.731284$  then the system has a single, stable stationary state  $(x_s, y_s)$  for which  $x_s < 4.12112$  and  $y_s < 24.7323$ . For  $I_0 > 1.64789$  the system has a single, stable stationary state  $(x_s, y_s)$  for which  $x_s > 12.928$  and  $y_s > 121.968$ . If

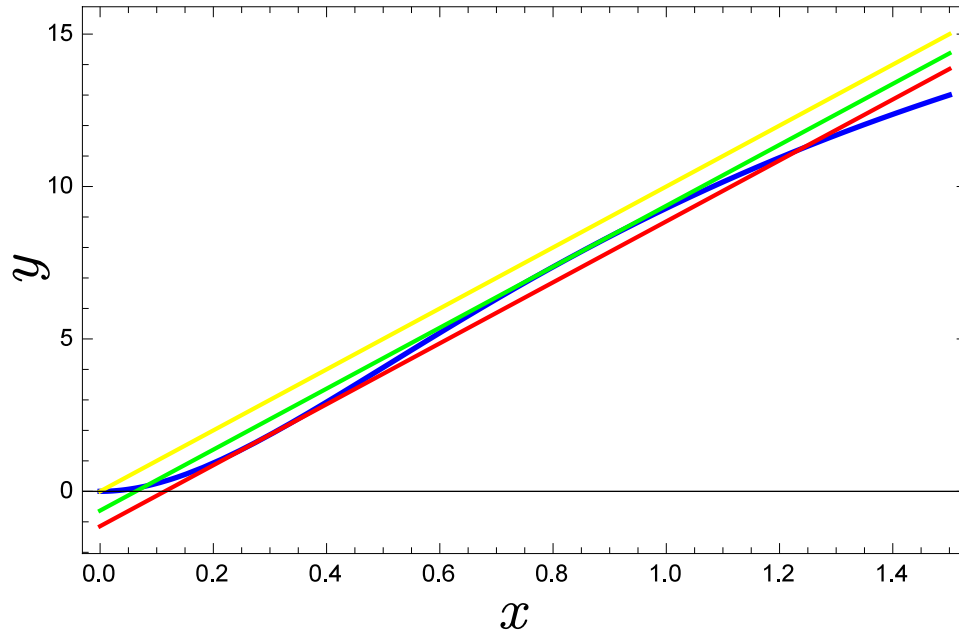


Figure 3.1 Positions of nullclines for the dynamical system defined by Eqs.(3.10,3.11) in the phase space  $(x, y)$ . The nullcline  $R(x, y) = 0$  is plotted with the blue line. The nullcline  $Q(x, y, t) = 0$  is shown for a few cases:  $I(t) \equiv 0$  (the orange line),  $I(t) \equiv 0.731284$  (the green line) and  $I(t) \equiv 1.64789$  (the red line). For the selected parameters of the model, the concentrations at tangential points are  $(x_1, y_1) = (4.12112, 24.7323)$  and  $(x_2, y_2) = (12.9281, 121.968)$

$0.731284 < I_0 < 1.64789$  then the system is bistable and shows hysteresis. Having in mind results of the previous chapter and the article [39] it is expected that a reaction in which an enzyme is activated by two control molecules can function as a discriminator of frequency and amplitude of a time dependent inflow.

In the following we consider periodic inflow described by the formula  $I(t) = A \cdot (\sin(2\pi\nu t + \phi_0) + 1) \cdot \Theta(t)$ . It is characterized by frequency  $\nu$  and the initial (for  $t = 0$ ) phase  $\phi_0$ . Such inflow term is always non-negative. The Heaviside step function describes the case where there is no inflow for  $t < 0$  and it is switched on at  $t = 0$ . If  $\phi_0 = 3 \cdot \pi/2$  then  $I(t)$  is a continuous function. In this case  $I(t = 0) = 0$ , next it increases and finally oscillates. For any other phase the inflow term is not continuous at  $t = 0$ ; for example if  $\phi_0 = \pi/2$  then  $I(t = 0) = 2 \cdot A$ , next  $I(t)$  decreases and oscillates later. For  $t > 0$  the time average of  $I(t)$  equals to  $A$  and it is independent of the frequency and the initial phase. If the inflow amplitude  $A = 0$  than  $(x = 0, y = 0)$  is a only steady state of Eqs.(3.10,3.11) and it is stable. We assume that this stable state is the initial state for the system evolution studied in numerical simulations.

Observations of changes in the character of oscillations in concentrations of reagents can be used to determine the frequency and amplitude of the inflow. Figure 2 illustrates the time evolution of concentration of  $Y$  for the fixed amplitude  $A = 1.2$  and a few different frequencies  $\nu = 0.0022, 0.00306, 0.00307, 0.00309, 0.0031$ . The solid line shows the time evolution calculated from the full reaction model described by Eqs.(6-9). The blue dashed line plots the time evolution for the reduced, two-variable model based on Eqs.(10,11). The full model of reaction and the reduced model are in a full agreement for low and high frequencies. Like in the previous chapter, for the lowest input frequency the oscillations of  $y(t)$  extend over a large range of concentrations. For high inflow frequencies the system oscillates below the tangential value  $y_2 = 121.968$ . In a narrow interval of frequencies the character of evolution significantly changes. Oscillations observed in  $y(t)$  switch from large values exceeding  $y_2$  to oscillations below this value. For the considered amplitude the full model predicts such transition for frequencies in the interval  $[0.00307, 0.00309]$ . The reduced model predicts that this transition occurs at slightly higher frequencies, in the interval  $[0.00309, 0.0031]$ . Therefore, as concluded in the previous chapter, from the observation of time evolution of concentration in the considered enzymatic system one can discriminate the frequency of the inflow, it the

amplitude of inflow is known.

Results shown in Fig. 2 illustrate that around the frequency that separates different oscillation types the medium needs some time before it reaches the steady form of oscillations. For the enzyme activation with two molecules we apply classification of the oscillation type is based on the minimum and maximum of  $y(t)$  observed in a long time interval for which the evolution has presumably reached its stationary character. Here we use  $t_{min} = 8000$  and  $t_{max} = t_{min} + 2000$  We introduce:

$$y_{min} = \min_{t \in [t_{min}, t_{max}]} y(t) \quad (3.12)$$

and

$$y_{max} = \max_{t \in [t_{min}, t_{max}]} y(t) \quad (3.13)$$

We distinguish oscillations on the upper stable branch (USB) of  $R(x, y) = 0$  nullcline if  $y_{min} > y_1 = 24.7323$  and  $y_{max} > y_2$  from oscillations on the lower stable branch (LSB). For those  $y_{min} < y_1$  and  $y_{max} < y_2$ .

The line separating USB from LSB oscillations in the phase space  $\nu, A$  is shown in Fig 3. The solid line corresponds to the full model, whereas symbols give results of the reduced model. For the selected values of reaction parameters the agreement between both models is very good. Our discrimination method is based on location of a given oscillation type with respect to the line separating USB for LSB oscillations. Let us denote points on this line as  $(\nu_c, A_c)$ . The frequency  $\nu_c$  treated as a function of  $A_c$  is an increasing function  $\nu_c = Z(A_c)$ . For example if we like to determine if the frequency of inflow  $\nu$  is higher than  $\nu_0$  then we should select the inflow amplitude equal to  $A = Z^{-1}(\nu_0)$  and observe the character of oscillations. If we observe USB oscillations then  $\nu < \nu_0$ . Observation of LSB oscillations indicates that  $\nu > \nu_0$ . The sensitivity of the method changes with the frequency  $\nu_0$ . In order to detect a high frequency inflow, the inflow amplitude should be selected with much higher precision than for  $0.005 \leq \nu_c \leq 0.01$ . One can also use the transition between class LSB and USB oscillations to determine the inflow amplitude. Unlike for frequency, the range of discriminated

amplitudes does not extend outside the interval  $[A_1/2, A_1]$ . If the amplitude  $A > A_1$  than, at a high frequency  $\nu$  the inflow of control molecules is close to the average inflow  $A$ . For such inflow the steady state of the system is located at USB and no transition between oscillation character is expected.

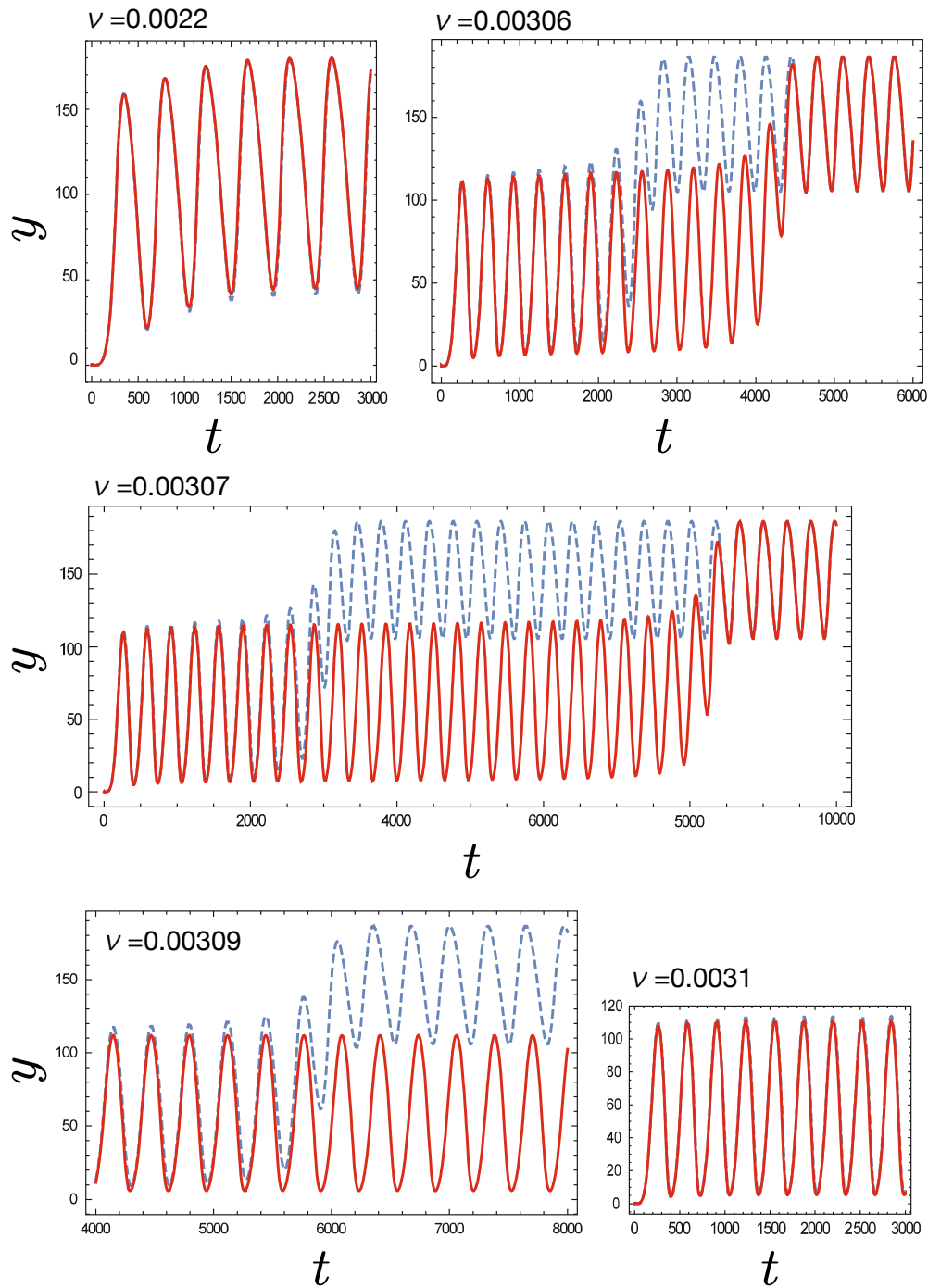


Figure 3.2 The concentration of  $Y$  as a function of time for the fixed amplitude  $A = 1.2$  and a few different frequencies ( $\nu = 0.0022, 0.00306, 0.00307, 0.00309, 0.0031$ ). The solid line shows the time evolution calculated from the full reaction model (Eqs.(6-9)). The blue dashed line plots the time evolution for the reduced, two-variable model based on Eqs.(3.10,3.11).

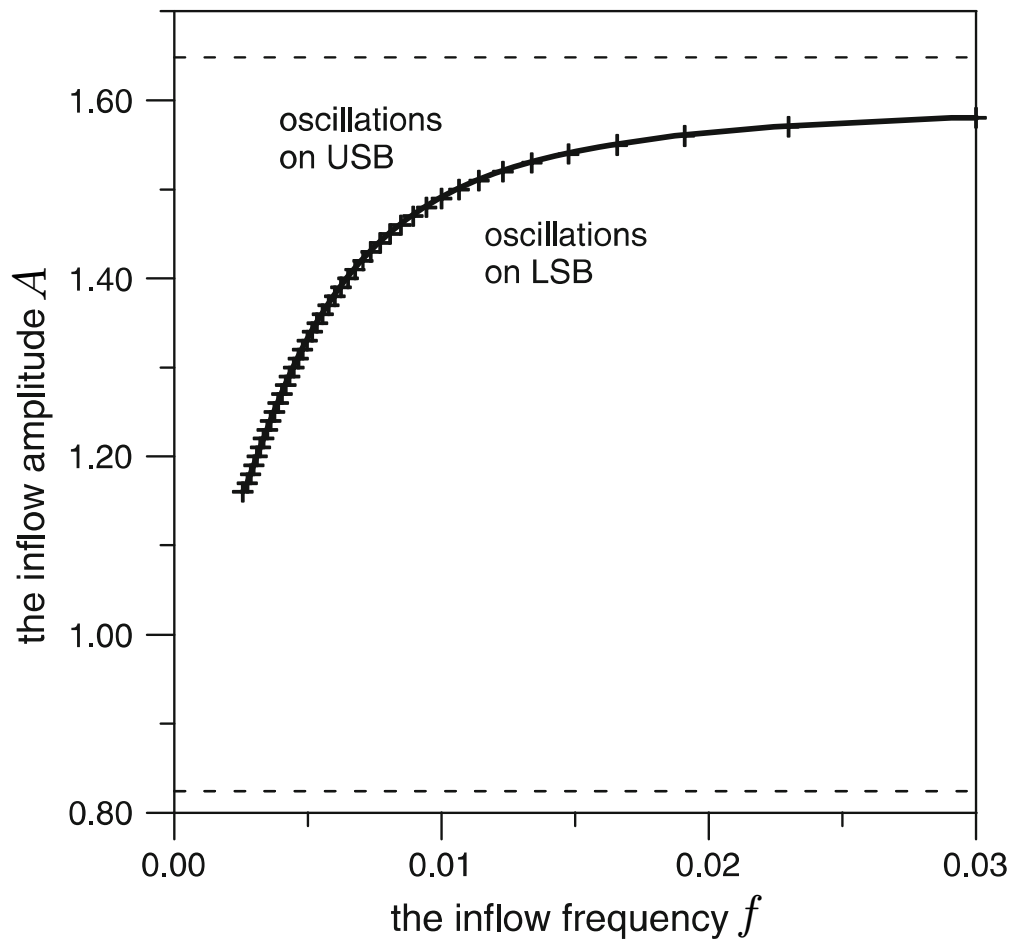
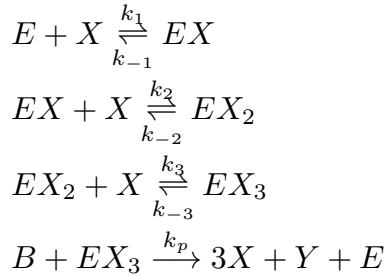


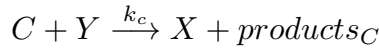
Figure3.3 The phase diagram showing the oscillation type as a function of inflow parameters  $(\nu, A)$ . The solid line corresponds to the full model, symbols give results of the reduced model. The horizontal dashed lines mark positions of  $A_1/2$  and  $A_1$ .

### 3.2.3 Enzyme activation with three control molecules

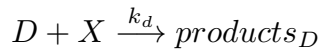
Finally, let us consider yet more complex reaction model in which the enzyme molecule  $E$  has to combine with three molecules of reagent  $X$  in order to transform the reactant  $B$  into the final product  $Y$ :



As in the previous case we assume that these reactions involving the enzyme  $E$  and its complexes are fast and lead to quasistationary concentrations of  $E$ ,  $EX$ ,  $EX_2$  and of  $EX_3$  (denoted as  $h(t)$ ). Moreover, like in the cases discussed before these reactions combine with slow processes:



and



Now the complete description of the system is given by five kinetic equations describing the time evolution of  $f(t)$ ,  $g(t)$ ,  $h(t)$ ,  $x(t)$  and  $y(t)$ :

$$\begin{aligned} \frac{dx(t)}{dt} = & -k_1e(t)x(t) + k_{-1}f(t) - k_2f(t)x(t) + k_{-2}g(t) - k_3g(t)x(t) + \\ & k_{-3}h(t) + 3k_pbh(t) - k_d x(t) + k_c cy(t) + I(t) \end{aligned} \quad (3.14)$$

$$\frac{df(t)}{dt} = k_1ex(t) - k_{-1}f(t) - k_2f(t)x(t) + k_{-2}g(t) \quad (3.15)$$

$$\frac{dg(t)}{dt} = k_2ex(t) - k_{-2}g(t) - k_3g(t)x(t) + k_{-3}h(t) \quad (3.16)$$

$$\frac{dh(t)}{dt} = k_3g(t)x(t) - k_{-3}h(t) - k_pbh(t) \quad (3.17)$$

$$\frac{dy(t)}{dt} = k_pbh(t) - k_c cy(t) \quad (3.18)$$

If we assume that concentrations of  $EX$ ,  $EX_2$  and  $EX_3$  complexes can be regarded as quasistationary ones then the model can be reduced to two kinetic equations for the time evolution of  $x(t)$  and  $y(t)$ :

$$\begin{aligned} \frac{dx(t)}{dt} &= Q(x(t), y(t), t) \\ &= -k_d dx(t) + k_c cy(t) + I(t) \end{aligned} \quad (3.19)$$

$$\begin{aligned} \frac{dy(t)}{dt} &= S(x(t), y(t)) \\ &= k_pbh(t) - k_c cy(t) \\ &= -k_c cy(t) + k_1k_2k_3k_p b^2 e_0 x^3(t) / \\ &\quad (k_{-1}k_{-2}k_{-3} + k_{-1}k_{-2}k_p b + k_1k_{-2}k_{-3}bx(t) + k_{-1}k_3k_p bx(t) + k_1k_{-2}k_p b^2 x(t) \\ &\quad + k_1k_2k_{-3}x^2(t) + k_1k_2k_p b^2 x^2(t) + k_1k_3k_p b^2 x^2(t) + k_2k_3k_p bx^2(t) \\ &\quad + k_1k_2k_3bx^3(t)) \end{aligned} \quad (3.20)$$

where  $e_0$  denotes the total concentration of enzyme in its free and all complexed forms ( $e_0 = e(t) + f(t) + g(t) + h(t) = const.$ ).

For the full reaction model it seems difficult to guess the values of parameters for which the model exhibits hysteresis and can be used to discriminate the amplitude or frequency of the inflow. It is easier to consider the reduced model and find reaction parameters leading to the sigmoidal shape of  $S(x, y) = 0$  nullcline. For example, such behaviour is observed when  $b = c = d = e_0 = 1$ , the rate constants for fast reactions are  $k_1 = 10, k_{-1} = 20, k_2 = 10, k_{-2} = 40, k_3 = 10, k_{-3} = 20, k_p = 15$  and the rate

constants for the slow reactions leading to products  $k_c = 1, k_d = 1$ . Figure 4 illustrates the nullclines for these values of parameters. The nullcline  $Q(x, y, t) = 0$  is shown for a few values of inflow:  $I(t) \equiv 0, I(t) \equiv 0.583234$  and  $I(t) \equiv 0.914414 = A_2$ . The last two values of inflow correspond to cases when the nullcline  $Q(x, y, t)$  is tangential to the nullcline  $S(x, y)$ . If the inflow  $I(t) < 0.583234$  then the system has a single, stable stationary state  $(x_s, y_s)$  for which  $x_s < 1.71818$  and  $y_s < 0.803767$ . If the inflow  $I(t) > 0.914414$  then the system has a single, stable stationary state  $(x_s, y_s)$  for which  $x_s > 4.39961$  and  $y_s > 3.81637$ . If the inflow does not depend on time after it is switched on ( $I(t) = I_0 \cdot \Theta(t)$ ) and  $0.583234 < I_0 < 0.914414$  then the system is bistable and shows hysteresis effect. Therefore, the reaction in which the enzyme is activated by three molecules can also function as a discriminator of inflow parameters.

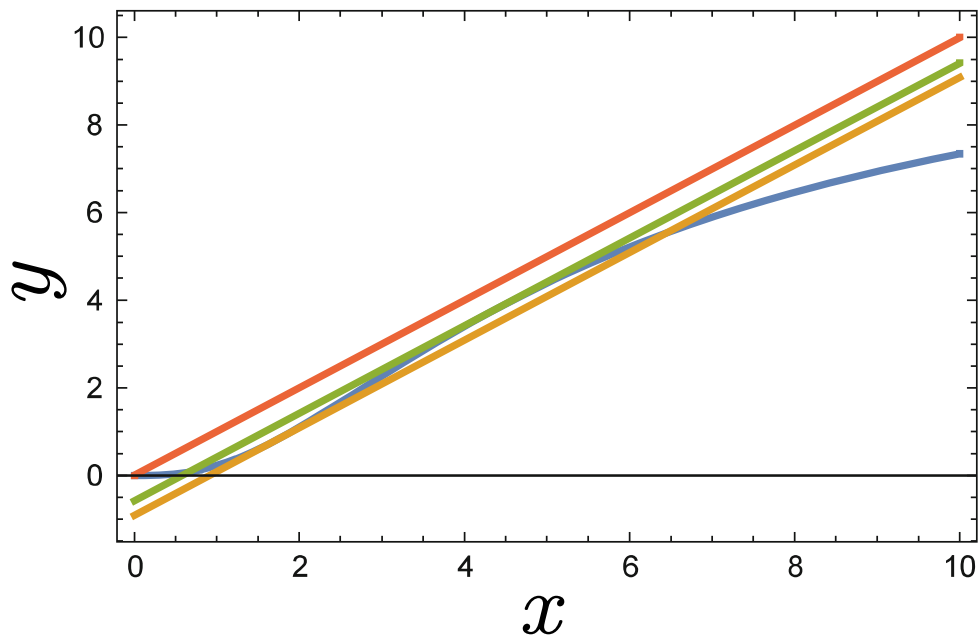


Figure 3.4 Positions of nullclines for the dynamical system defined by Eqs.(3.19,3.20) in the phase space  $(x, y)$ . The nullcline  $S(x, y) = 0$  is plotted with the blue line. The nullcline  $Q(x, y, t) = 0$  is shown for a few cases:  $I(t) \equiv 0$  (the red line),  $I(t) \equiv 0.583234$  (the green line) and  $I(t) \equiv 0.914414$  (the orange line). For the selected parameters of the model, the concentrations at tangential points are  $(x_1, y_1) = (1.71818, 0.803767)$  and  $(x_2, y_2) = (4.39961, 3.81637)$ .

Like in the previous case we consider the periodic inflow of  $X$  with the frequency  $\nu$  and the initial phase  $\phi_0$  described by the expression:  $I(t) = A \cdot (\sin(2\pi\nu t + \phi_0) + 1) \cdot \Theta(t)$ . The the initial state for numerical simulations is always  $(x = 0, y = 0)$ , because it is the only stable state when  $I(t) \equiv 0$ . In order to classify oscillations we calculate  $y_{min}$  and  $y_{max}$  according to Eqs.(3.12,3.13) for  $t_{min} = 1000$  and  $t_{max} = 2000$ . Yet again we distinguish states on the upper stable branch (USB) of  $S(x, y) = 0$  nullcline if  $y_{min} > y_2 = 3.81637$  and oscillations on the lower stable branch (LSB) for which  $y_{max} < y_2$ .

Figure 5 illustrates the time evolution of concentration of  $Y$  for the fixed amplitude  $A = 0.8$  and six different frequencies  $\nu = 0.01, 0.015, 0.023, 0.024, 0.0282$  and  $0.0284$ . Like in Fig. 2 for low frequencies the oscillations of  $y(t)$  extend over a large interval of concentrations. For higher frequencies the system exhibit USB oscillations. If the frequency of inflow  $\nu$  exceeds a critical value LSB oscillations appear. The LSB oscillations remain stable at high frequencies. Qualitatively the same scenario is seen for both full and the reduced model. The fact that transition between two types of oscillations occurs in a narrow range of frequencies indicates that the considered enzymatic reaction can be also applied for discrimination of the inflow parameters.

Unlike for the enzyme activated by two molecules of  $X$  we observe significant quantitative differences between the full and the reduced models. For  $A = 0.8$  the time evolutions predicted by both models are in perfect agreement for  $\nu = 0.01$ , however at higher frequencies results differ. The full model predicts the transition between USB and LSB oscillations in the interval  $[0.023, 0.24]$ , whereas the reduced models places this transition at higher frequencies in the interval  $[0.0282, 0.284]$ . We believe that the difference comes from a high inflow frequency for which quasistationariy of the enzyme complexes does not hold.

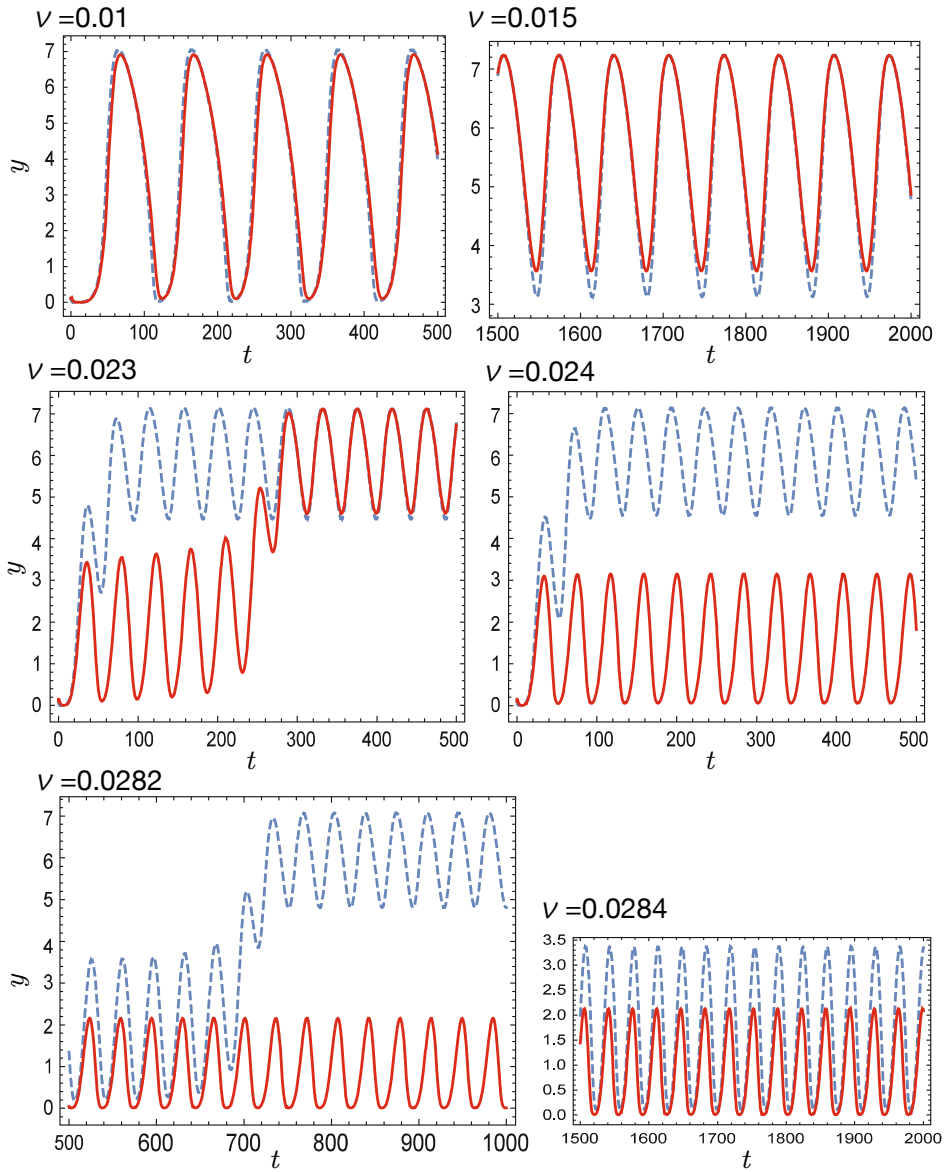


Figure 3.5 The concentration of  $Y$  as a function of time for the model in which the enzyme molecule is activated by three molecules of reagent. Results are presented for a fixed amplitude  $A = 0.8$  and a few selected inflow frequencies  $\nu$ , given above corresponding figures. The initial phase is  $\phi_0 = 3\pi/2$  for all cases. The red solid line shows the time evolution calculated from the full reaction model ( Eqs.(3.14-3.18)). The blue dashed line plots the time evolution for the reduced, two-variable model based on Eqs.(3.19,3.20)

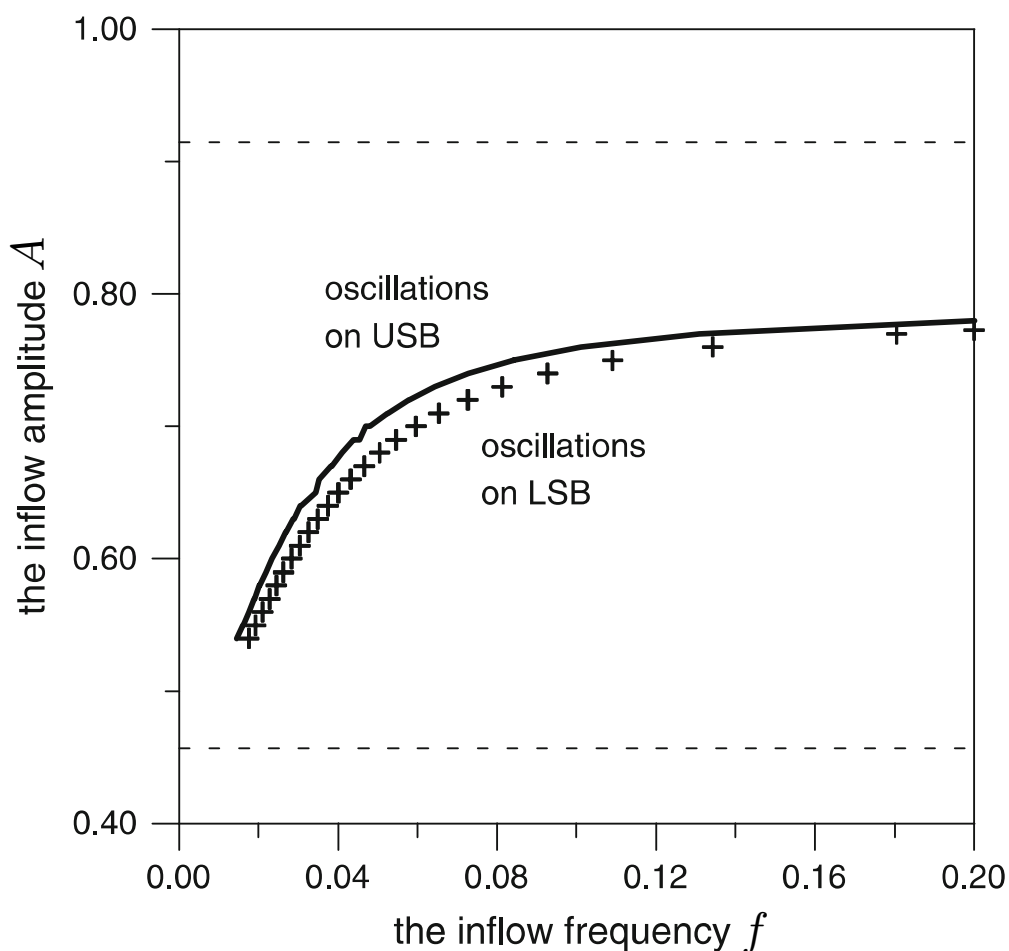


Figure 3.6 The phase diagram showing the oscillation type as a function of inflow parameters  $(\nu, A)$ . The solid line corresponds to the full model; the symbols give results of the reduced model. The horizontal dashed lines mark positions of  $A_1/2$  and  $A_1$ .

Fig. 6 illustrates the regions of parameters  $(\nu, A)$  for which a given oscillation pattern is observed. The solid line corresponds to the full model and symbols give results of the reduced model. The agreement between models at low frequencies is good but the results diverge when  $\nu$  increases. Therefore, the reduced model can be used for qualitative studies of transition between different oscillation types and the full reaction model has to be used to calculate the line separating different oscillation types. Like in the previous case the accuracy of frequency determination decreases as a function of frequency.

### 3.3 Conclusions

In this report we presented two models of an enzymatic reaction that can be applied for unconventional information processing as discriminators of input parameters. We have demonstrated that reaction models in which the enzyme is activated by two or three control molecules show hysteresis if the model parameters are properly selected. Therefore, the reactions can be used for a novel discrimination strategy described in [39]. This discrimination strategy has been originally introduced for a formal model of dynamical system. According to it the information about the amplitude and frequency of the inflow can be obtained by observation of oscillations in reagent concentration. Here we confirmed that the strategy applies to realistic models of chemical reactions.

There are many parameters (rate constants, concentrations of reagents in excess) in the considered reaction models. Depending on the model a state of system is described by concentrations of 4 or 5 reagents. Therefore, a straightforward identification of parameter values, at which the reaction can be used as a discriminator seems difficult. Here we restricted our attention to the cases in which reactions involving the enzyme and its complexes are faster than the other processes. We reduced the full reaction model to two kinetic equations. In the reduced model one of the nullclines has a sigmoidal form. Using the arguments given in [39] one can easily estimate the range of input frequency or amplitude in which a sharp transition between different forms of oscillations, necessary for discrimination, is observed. The comparison of results shows a qualitative agreement between the full reaction model and the reduced one. For the reaction with enzyme activation by two control molecules we have also found a good quantitative agreement between the models. In the other case (enzyme activation by three control molecules) we observed significant differences in the inflow amplitude and frequency at which the transition between different forms of oscillations occurs. Therefore, although the strategy of discrimination can be easily explained for two-variable model with a sigmoidal nullcline, precise calculations of discriminator characteristics should be based on

the detailed reaction model. which provides more realistic interpretation to the dynamic response.

### 3.4 Acknowledgement

This work was supported by KAKENHI Grants-in-Aid for Scientific Research (15H02121, 25103012).

## References

- <sup>1</sup>A. Henson, J. M. P. Gutierrez, T. Hinkley, S. Tsuda and L. Cronin, 'Towards heterotic computing with droplets in a fully automated droplet-maker platform', *Philosophical Transactions of the Royal Society A: Mathematical, Physical and Engineering Sciences* **373**, 20140221 (2015).
- <sup>2</sup>J. Górecki, K. Giżyński, J. Guzowski, J. N. Górecka, P. Garstecki, G. Gruenert and P. Dittrich, 'Chemical computing with reaction-diffusion processes', *Philosophical Transactions of the Royal Society A: Mathematical, Physical and Engineering Sciences* **373**, 20140219 (2015).
- <sup>3</sup>C. L. Nehaniv, J. Rhodes, A. Egri-Nagy, P. Dini, E. R. Morris, G. Horváth, F. Karimi, D. Schreckling and M. J. Schilstra, 'Symmetry structure in discrete models of biochemical systems: natural subsystems and the weak control hierarchy in a new model of computation driven by interactions', *Philosophical Transactions of the Royal Society A: Mathematical, Physical and Engineering Sciences* **373**, 20140223 (2015).
- <sup>4</sup>A. Adamatzky, 'Slime mould processors, logic gates and sensors', *Philosophical Transactions of the Royal Society A: Mathematical, Physical and Engineering Sciences* **373**, 20140216 (2015).
- <sup>5</sup>E. Katz, ed., *Biomolecular Information Processing: From Logic Systems to Smart Sensors and Actuators* (Wiley-VCH Verlag GmbH & Co. KGaA, Weinheim, Germany, 4th July 2012).
- <sup>6</sup>E. Katz, ed., *Molecular and Supramolecular Information Processing: From Molecular Switches to Logic Systems* (Wiley-VCH Verlag GmbH & Co. KGaA, Weinheim, Germany, 4th July 2012).
- <sup>7</sup>K. Szaciłowski, 'Digital Information Processing in Molecular Systems', *Chemical Reviews* **108**, 3481–3548 (2008).
- <sup>8</sup>U. Pischel, J. Andréasson, D. Gust and V. F. Pais, 'Information Processing with Molecules—Quo Vadis?', *ChemPhysChem* **14**, 28–46 (2013).

- <sup>9</sup>T. R. Head, G. Rozenberg, R. Bladergroen, C. K. Breek, P. H. Lommerse and H. P. Spaink, ‘Computing with DNA by operating on plasmids’, *Biosystems* **57**, 87–93 (2000).
- <sup>10</sup>T. Head, X. Chen, M. Yamamura and S. Gal, ‘Aqueous computing: A survey with an invitation to participate’, *Journal of Computer Science and Technology* **17**, 672 (2002).
- <sup>11</sup>Y. Benenson, ‘Biocomputers: from test tubes to live cells’, *Molecular BioSystems* **5**, 675–685 (2009).
- <sup>12</sup>M. N. Stojanovic, D. Stefanovic and S. Rudchenko, ‘Exercises in Molecular Computing’, *Accounts of Chemical Research* **47**, 1845–1852 (2014).
- <sup>13</sup>S. Mailloux, Y. V. Gerasimova, N. Guz, D. M. Kolpashchikov and E. Katz, ‘Bridging the Two Worlds: A Universal Interface between Enzymatic and DNA Computing Systems’, *Angewandte Chemie International Edition* **54**, 6562–6566 (2015).
- <sup>14</sup>V. Privman, O. Zavalov, L. Halámková, F. Moseley, J. Halánek and E. Katz, ‘Networked Enzymatic Logic Gates with Filtering: New Theoretical Modeling Expressions and Their Experimental Application’, *The Journal of Physical Chemistry B* **117**, 14928–14939 (2013).
- <sup>15</sup>A. Hjelmfelt, E. D. Weinberger and J. Ross, ‘Chemical implementation of neural networks and Turing machines’, *Proceedings of the National Academy of Sciences* **88**, 10983 (1991).
- <sup>16</sup>A. Hjelmfelt, E. D. Weinberger and J. Ross, ‘Chemical implementation of finite-state machines’, *Proceedings of the National Academy of Sciences* **89**, 383 (1992).
- <sup>17</sup>A. Hjelmfelt and J. Ross, ‘Mass-coupled chemical systems with computational properties’, *The Journal of Physical Chemistry* **97**, 7988–7992 (1993).
- <sup>18</sup>A. Hjelmfelt and J. Ross, ‘Implementation of logic functions and computations by chemical kinetics’, *Dynamism and Regulation in Nonlinear Chemical Systems* **84**, 180–193 (1995).
- <sup>19</sup>A. Arkin and J. Ross, ‘Computational functions in biochemical reaction networks’, *Biophysical Journal* **67**, 560–578 (1994).

- <sup>20</sup>E. Katz and V. Privman, ‘Enzyme-based logic systems for information processing’, *Chemical Society Reviews* **39**, 1835–1857 (2010).
- <sup>21</sup>V. Privman, J. Halánek, M. A. Arugula, D. Melnikov, V. Bocharova and E. Katz, ‘Biochemical Filter with Sigmoidal Response: Increasing the Complexity of Biomolecular Logic’, *The Journal of Physical Chemistry B* **114**, 14103–14109 (2010).
- <sup>22</sup>M. Pita, V. Privman, M. A. Arugula, D. Melnikov, V. Bocharova and E. Katz, ‘Towards biochemical filters with a sigmoidal response to pH changes: buffered biocatalytic signal transduction’, *Physical Chemistry Chemical Physics* **13**, 4507–4513 (2011).
- <sup>23</sup>S. Domanskyi and V. Privman, ‘Design of Digital Response in Enzyme-Based Bioanalytical Systems for Information Processing Applications’, *The Journal of Physical Chemistry B* **116**, 13690–13695 (2012).
- <sup>24</sup>V. Privman, B. E. Fratto, O. Zavalov, J. Halánek and E. Katz, ‘Enzymatic AND Logic Gate with Sigmoid Response Induced by Photochemically Controlled Oxidation of the Output’, *The Journal of Physical Chemistry B* **117**, 7559–7568 (2013).
- <sup>25</sup>R. A. Laskowski, F. Gerick and J. M. Thornton, ‘The structural basis of allosteric regulation in proteins’, *FEBS Letters* **583**, 1692–1698 (2009).
- <sup>26</sup>T. Tsuruyama, T. Nakamura, G. Jin, M. Ozeki, Y. Yamada and H. Hiai, ‘Constitutive activation of Stat5a by retrovirus integration in early pre-B lymphomas of SL/Kh strain mice’, *Proceedings of the National Academy of Sciences* **99**, 8253–8258 (2002).
- <sup>27</sup>T. Tsuruyama, ‘A Model of Cell Biological Signaling Predicts a Phase Transition of Signaling and Provides Mathematical Formulae’, *PLOS ONE* **9**, e102911 (2014).
- <sup>28</sup>K.-P. Zauner and M. Conrad, ‘Enzymatic Computing’, *Biotechnology Progress* **17**, 553–559 (2001).
- <sup>29</sup>S. Bakshi, O. Zavalov, J. Halánek, V. Privman and E. Katz, ‘Modularity of Biochemical Filtering for Inducing Sigmoid Response in Both Inputs in an Enzymatic AND Gate’, *The Journal of Physical Chemistry B* **117**, 9857–9865 (2013).

- <sup>30</sup>J. D. Rabinowitz, J. J. Hsiao, K. R. Gryncel, E. R. Kantrowitz, X.-J. Feng, G. Li and H. Rabitz, 'Dissecting Enzyme Regulation by Multiple Allosteric Effectors: Nucleotide Regulation of Aspartate Transcarbamoylase', *Biochemistry* **47**, 5881–5888 (2008).
- <sup>31</sup>H. C. Barrett, 'Enzymatic Computation and Cognitive Modularity', *Mind & Language* **20**, 259–287 (2005).
- <sup>32</sup>J. Halánek, O. Zavalov, L. Halámková, S. Korkmaz, V. Privman and E. Katz, 'Enzyme-Based Logic Analysis of Biomarkers at Physiological Concentrations: AND Gate with Double-Sigmoid "Filter" Response', *The Journal of Physical Chemistry B* **116**, 4457–4464 (2012).
- <sup>33</sup>O. Zavalov, V. Bocharova, V. Privman and E. Katz, 'Enzyme-Based Logic: OR Gate with Double-Sigmoid Filter Response', *The Journal of Physical Chemistry B* **116**, 9683–9689 (2012).
- <sup>34</sup>R. Baron, O. Lioubashevski, E. Katz, T. Niazov and I. Willner, 'Elementary Arithmetic Operations by Enzymes: A Model for Metabolic Pathway Based Computing', *Angewandte Chemie International Edition* **45**, 1572–1576 (2006).
- <sup>35</sup>H. Lederman, J. Macdonald, D. Stefanovic and M. N. Stojanovic, 'Deoxyribozyme-Based Three-Input Logic Gates and Construction of a Molecular Full Adder', *Biochemistry* **45**, 1194–1199 (2006).
- <sup>36</sup>J. Górecki, J. N. Górecka, K. Yoshikawa, Y. Igarashi and H. Nagahara, 'Sensing the distance to a source of periodic oscillations in a nonlinear chemical medium with the output information coded in frequency of excitation pulses', *Physical Review E* **72**, 046201 (2005).
- <sup>37</sup>K. Yoshikawa, H. Nagahara, T. Ichino Takatoshi, J. Górecki, J. N. Górecka and Y. Igarashi, 'On chemical methods of direction and distance sensing', *International Journal of Unconventional Computing* **5**, 53–65 (2009).
- <sup>38</sup>M. Tanaka, H. Nagahara, H. Kitahata, V. Krinsky, K. Agladze and K. Yoshikawa, 'Survival versus collapse: Abrupt drop of excitability kills the traveling pulse, while gradual change results in adaptation', *Physical Review E* **76**, 016205 (2007).

- <sup>39</sup>H. Ueno, T. Tsuruyama, B. Nowakowski, J. Górecki and K. Yoshikawa, ‘Discrimination of time-dependent inflow properties with a cooperative dynamical system’, *Chaos: An Interdisciplinary Journal of Nonlinear Science* **25**, 103115 (2015).
- <sup>40</sup>M. A. Krasnosel’skii and A. V. Pokrovskii, *Systems with Hysteresis* (Springer-Verlag, Berlin Heidelberg, 1989).
- <sup>41</sup>М. А. Красносельский and А. В. Покровский, *Системы с гистерезисом* (Наука, 1983).
- <sup>42</sup>J. D. Murray, *Mathematical biology*, 3rd ed, Vol. 17, *Interdisciplinary Applied Mathematics* (Springer, New York, 2002), 2 pp.
- <sup>43</sup>S. Goutelle, M. Maurin, F. Rougier, X. Barbaut, L. Bourguignon, M. Ducher and P. Maire, ‘The Hill equation: a review of its capabilities in pharmacological modelling’, *Fundamental & Clinical Pharmacology* **22**, 633–648 (2008).

## Chapter 4

# Emergence of Many Mini-Circles from a Coffee Suspension with Mechanical Rotation

### 4.1 Introduction

The formation of a deposition pattern with the evaporation of a liquid containing non-volatile particles has attracted considerable interest not only from a fundamental scientific aspects perspective [1–3], but also from an engineering point of view with respect to coating and patterning processes [4, 5]. As a typical pattern, a so-called coffee-ring is caused by the transportation of solute particles toward a pinned contact line driven by Marangoni effect, or spatial gradient of the surface tension, under a differential evaporation rate over the liquid/air surface [6–11]. In addition to the formation of a ring-like pattern [12], the generation of various kinds of morphologies, such as fractures, cracks, straight lines, spiral and dry parch, have been reported in the drying of droplets containing micro or nanoparticles [13–22]. Smart control of the positioning of nanoparticles by using photo-sensitive surfactant in drying droplets was also reported [23]. It has

been shown that particles can be concentrated at the center of a droplet through spot-irradiation of its apex with a heating laser, by dismissing the coffee-ring pattern, which phenomenon was interpreted in terms of the reversal of intra-droplet flow induced by a thermal Marangoni effect [24, 25]. A similar manner of particle deposition at the center of a droplet was observed when the solvent was changed from water to octane [26]. To suppress the coffee-ring effect, or the heterogeneous deposition of particles, various methodologies have been proposed, including the application of a surface acoustic wave [27], the imposition of electronic fields [28, 29], heating of the solid substrate [30], and the addition of a surfactant [31, 32]. In the present study, we performed a drying experiment by adopting an aqueous suspension containing fine coffee powder/granules, i.e., Turkish coffee, which is usually served without filtering and thus contains a relatively large amount of micro-particles. Drying this solution under a horizontal static condition results in the formation of a homogeneous granular layer without the formation of a coffee-ring. Interestingly, characteristic patterns of drying granules, such as multiple wavy segments and several mini-circles, are generated using a rotating dish under a tilting condition.

## 4.2 Materials and Methods

Roasted coffee beans were ground with a conical burr coffee grinder (product MSCS-2B, Hario Co. Ltd., Tokyo, Japan). Larger particles were sieved out of the ground powder with a sifter (grid size of 250  $\mu\text{m}$ , Tokyo Screen Co., Ltd., Tokyo, Japan). In Figure 1, the experimental procedure in a schematic manner is shown, together with the photograph of the coffee powder (average diameter of 68  $\mu\text{m}$ , and standard deviation of 23  $\mu\text{m}$ ). Aqueous solution was prepared by mixing 900 mg of ground coffee beans with 3 mL of ultrapure water (produced with Milli-Q water purification system, Millipore, Merck). The mixed solution was transferred onto a paper dish, of which the surface laminated with polyethylene terephthalate is hydrophobic and the diameter of the bottom planar part is 140 mm (RS-362, Dixie Japan Ltd., Tokyo, Japan). Then, the solution

was mechanically homogenized with a vortex mixer (SI-0286, Scientific Industries Inc., Bohemia, NY, USA). In the present Communication, we report the experimental results under the conditions that the paper dish was fixed to a rotating dish with a tilting angle of  $\theta = 45^\circ$  and was rotated at 60 rpm by a direct current motor (mini-motor multi-ratio gearbox (12-speed), item 70190, Tamiya Ltd., Tokyo, Japan). As for the effect of tilting, we found that the coffee solution tends to flow out from the dish when  $\theta$  is larger than  $60^\circ$ , whereas contrast of the generating pattern becomes relatively unclear when  $\theta$  is smaller than  $30^\circ$ . Thus, we have carried out the experiment by taking the tilting angle as  $45^\circ$ . Under the condition  $\theta = 45^\circ$ , when the rotation rate is smaller than 30 rpm, the solution tends to flow downward outside the dish. When the rotation rate is larger than 100 rpm, the generated pattern tends to be inhomogeneous between the inner and outer regions of the dish, because of the relatively large magnitude of the oscillation on the centrifugal force. Based on the results of these preliminary experiments, we report the experimental results at the fixed values of the tilting angle at  $45^\circ$  and rotational rate at 60 rpm, in order to reveal the representable transition of the drying patterns between wavy fragmented stripes and many mini-circles.

### 4.3 Results and Discussion

Figure 4.3 shows the drying patterns obtained from the coffee solution, by adopting (a–d) a solution containing coffee powder (see Figure 4.2a) and (e) filtered solution without powder. All of the pictures were taken for the completely dried states after standing still for 24 h with horizontal positioning. For the experiments shown in (a–d), we used a suspension with the solution of coffee powder on a paper dish, of which the surface is hydrophobic. Figure 2a shows the appearance of a pattern with many wavy shapes, which was obtained by fixing the solution on the tilted plate for 10 s in a stationary manner and then rotating it for 1 min. Hereafter, we call this morphology a “waggly” pattern. Figure 2b shows the drying pattern after 10 s of stationary tilting and then 20 min of plate rotation. The appearance of many mini-circles with a diameter of  $\sim 1$

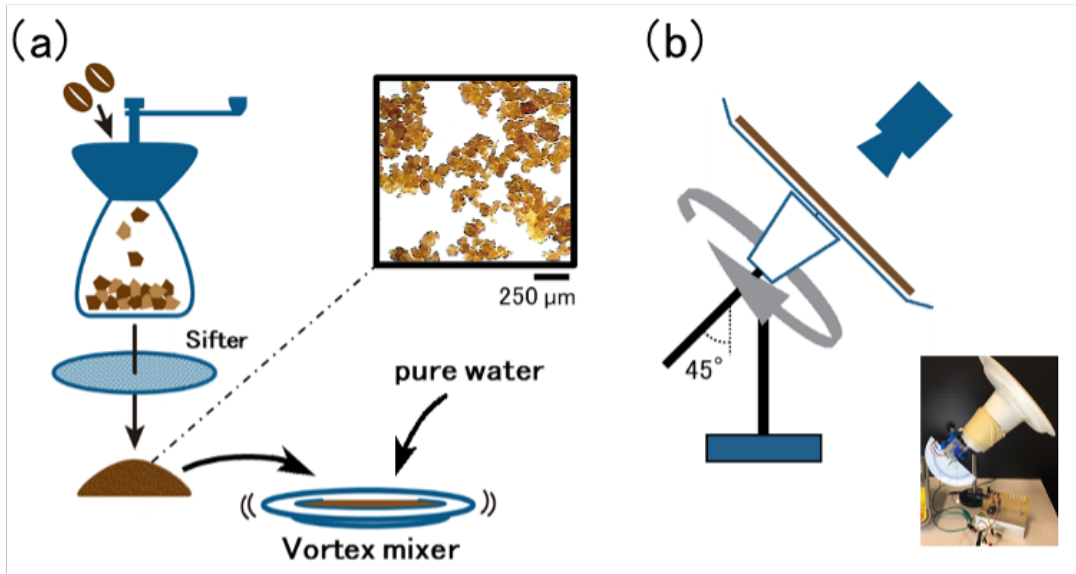


Figure 4.1 Experimental scheme. (a) Roasted coffee beans were ground with a conical burr grinder. Larger particles were sieved out of the ground powder with a sifter (grid size:  $250\ \mu\text{m}$ ). The ground coffee was mixed with pure water on a paper dish (diameter of the horizontal circular area:  $140\ \text{mm}$ ), and the solution was spread over the whole dish by vibration with a vortex mixer. (b) Experimental apparatus to rotate the tilted dish with the solution containing the coffee particles. The paper dish with the coffee solution was fixed to a rotating dish with a tilting angle of  $\theta = 45^\circ$ . The dish was rotated at 60 rpm. During rotation, the whole experimental apparatus was situated inside a control box with constant humidity (60%) and temperature ( $20^\circ\text{C}$ ).

mm is observed, which we call “polka-dot” in this article. Here, it is to be noted that the waggly and polka-dot patterns appeared for the same experimental solution with different time-period of the dish rotation. Figure 2c shows a tree-like pattern which was generated under the stationary tilt condition for 1 min without rotation. Figure 2d shows a homogeneous layer of powder obtained by drying the coffee suspension under a horizontal arrangement. For comparison, Figure 2e shows a so-called coffee-ring, which was generated under horizontal drying of a droplet of coffee solution prepared through filtration. In both Figure 2d,e, 0.1 mL of coffee solution was deposited on the paper plate.

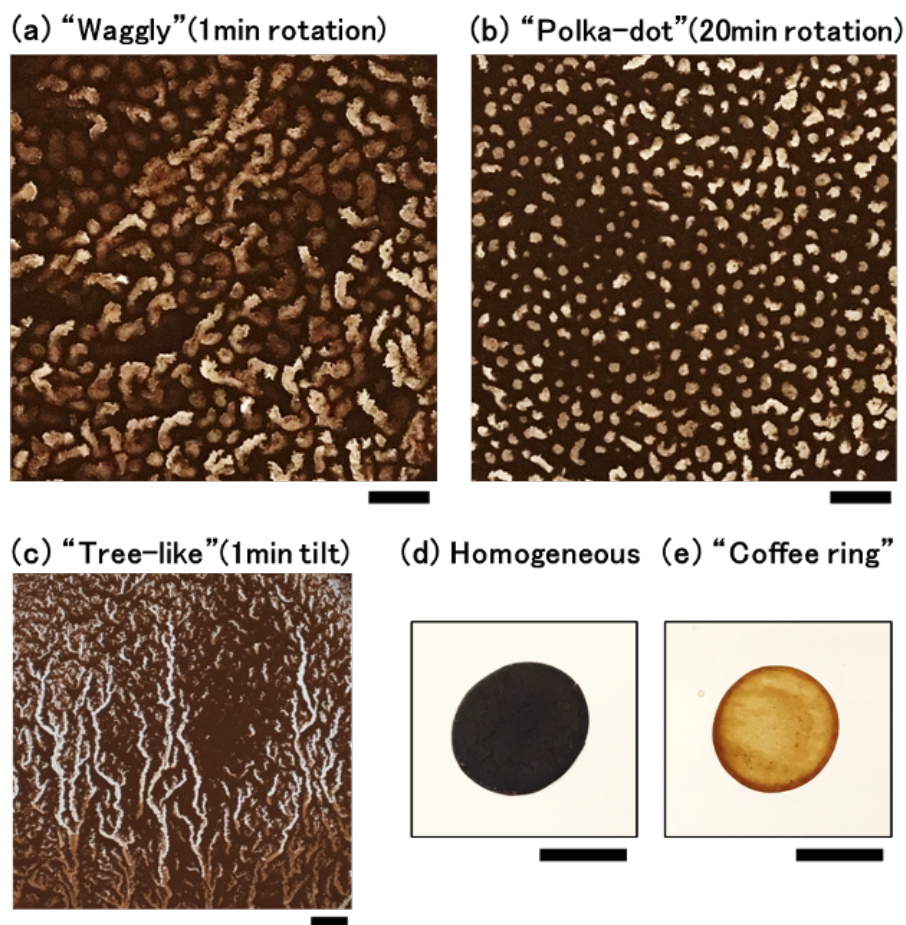


Figure 4.2 Generation of various characteristic patterns from a drying solution containing coffee powder under different conditions. The scale bars are 10 mm. **(a)** A waggly pattern with many wavy shapes formed when the paper dish was tilted while stationary for 10 s and then rotated for 1 min at a fixed angle of  $45^\circ$  (see Figure 1b). After the rotation, the dish was stood still horizontally for 24 h. The light brown and dark brown parts indicate water-rich and powder-rich regions, respectively. **(b)** Polka-dot pattern with many mini-circles generated from the coffee solution, with tilting without rotation for 10 s and then rotation for 20 min. After the rotation, the dish was stood still horizontally for 24 h. **(c)** Tree-like pattern caused by the downward flow of coffee solution when the plate was tilted at a fixed angle of  $45^\circ$  for 1 min without rotation, the dish was stood still horizontally for 24 h. **(d)** Homogeneous pattern formed by drying the coffee solution containing the powder, i.e., essentially the same solution as in a–c. **(e)** Usual so-called coffee-ring formed by drying the filtered coffee solution with almost no grained powder.

As shown in the experimental observations (Figure 2), it has become clear that drying under tilted rotation strongly affects the outcome; a waggly pattern appears first and then a polka-dot pattern develops. Next, we discuss the mechanism of the occurrence of the characteristic patterns. Under dish rotation, the coffee suspension is segregated into grain-rich and water-rich solutions as revealed in Figure 2. It would be expected that the underlying mechanism of the pattern formation observed for the suspension could be interpreted in terms of a kinetic effect in the first-order phase-transition. Thus, we will consider the appearance of the waggly and polka-dot patterns by adopting Cahn–Hilliard-type simple model equations [33–39]:

$$\frac{\partial \eta}{\partial t} = \nabla \left( M_c \nabla \frac{\delta F}{\delta \eta} \right), \quad (4.1)$$

where the free energy  $F$  exhibits two different contributions: bimodality with the order parameter and the interfacial energy. Here,  $M_c$  is a parameter of diffusivity and  $t$  is time.

$$F = \int \left( L\eta(1 - \eta) + \frac{\alpha}{2} |\nabla \eta|^2 \right) dv, \quad (4.2)$$

where  $L$ ,  $\alpha$  and  $dv$  are interaction parameter, gradient energy coefficient and differential volume, respectively. For simplicity, we chose the bimodal profile of the interaction energy as a function of  $\eta$ , corresponding to the water content in the solution containing coffee grains;  $\eta = 1$  corresponds to pure water. We also neglected the contribution from the mixing entropy, since we are considering the segregation of relatively large particles of coffee grains. For the calculation of Equation (2), we tentatively adopted the parameters  $L = 6.4 \times 10^3$  J/mol and  $\alpha = 3.0 \times 10^{-3}$  Jm<sup>2</sup>/mol, so as to obtain the pattern with usual spinodal decomposition. We may regard that  $\eta = 0, 1$  correspond to the dense coffee grains and the clear solution, respectively. Strictly speaking, our experimental system is non-conservative, because of the evaporation of water to cause the spatial pattern. Thus, the usual Cahn–Hilliard equation does not hold in a strict manner for our experiments, especially for the experimental conditions with relatively large effect of

the evaporation. However, the numerical results can still be expected to provide useful insight into the mechanism of pattern formation. Actually, for the initial stage of the drying process when the water content does not decrease so much, the kinetic equation based on Cahn–Hilliard model would represent the essential feature of the segregation. Since the order parameter  $\eta$  is dependent primarily on the relative concentration of the coffee grains, we may need to consider that the diffusivity  $M_c$  is sensitively dependent on  $\eta$ , in addition to the bimodal dependence (the term  $\eta(1 - \eta)$ ),

$$M_c = \left[ \frac{D_0}{RT}\eta + \frac{D_1}{RT}(1 - \eta) \right] \eta(1 - \eta), \quad (4.3)$$

where  $D_0$  and  $D_1$  are the diffusion constants for the states with  $\eta = 0$  and 1, respectively. In the following simulation, we used the universal gas constant  $R = 8.31 J/mol \cdot K$ . We adopted the apparent diffusion constants  $D_0 = 4.0 \times 10^{-10} \text{ m}^2/\text{s}$  and  $D_1 = 4.0 \times 10^{-8} \text{ m}^2/\text{s}$ , by taking into account the effect of the smaller diffusivity of the grain rich solution. We adapted one-order larger value for the apparent diffusivity of water,  $D_1$ , as that of the pure water with stationary standing state [40], by considering the effect owe to the rhythmic change in gravitational field induced by the dish rotation. As for the diffusivity of the grain powder (the diameter is ca.  $40 \mu\text{m}$  as estimated from the average diameter of  $68 \mu\text{m}$ , as mentioned in Materials and Methods), it is expected that its diffusion constant is on the order of  $10^{-5} - 10^{-6}$  compared to that of water for the usual Brownian motion under thermal equilibrium, as estimated from the Stokes–Einstein relationship. In addition, with the decrease of the water content, the diffusion of the coffee grain should become much lower. Thus, it is noted that the adapted value for  $D_1$  is rather large compared to the intrinsic diffusivity under the fluctuation-dispersion relationship near thermal equilibrium. In other words, we perform the numerical modeling with the consideration of the effect induced by the external agitation, i.e., the periodic change of the gravitational field accompanied by the rotation of the tilted dish. Through such simple assumptions, we performed a numerical simulation using a two-dimensional system to shed light on the essential mechanism on the time-development of the generated

pattern. It may be possible to include the effect of the periodic acceleration during dish rotation by tuning the effective temperature in the simulation. However, in the present study, for simplicity we used room temperature,  $T = 293$  K. We carried out the numerical simulation by modifying the source code of Python available from the open access version[41], provided by the “Yamanaka Laboratory” at Tokyo University of Agriculture and Technology, Japan. The grid spacing in the computation is taken as  $1.0 \times 10^{-3}$  m. The time width and step number are 0.01 s and 13,000, respectively; corresponding to a time-period of 130 s. Figure 3 exemplifies the segregation pattern generated after 130 s from the start of the segregation in the simulation. Figure 3a shows the appearance of wavy short-fragmented stripes, where the coloring of the segregation pattern is carried out with a threshold value of  $\eta = 0.53$ . This wavy pattern is familiar for phase segregation with spinodal decomposition[42] and apparently is similar to the waggly pattern observed in the early state (1 min rotation) of the drying process with vessel rotation as in Figure 2a. In contrast, Figure 3b shows the appearance of many mini-circles when the threshold is  $\eta = 0.56$ , corresponding to the polka-dot pattern observed in the late stage with rotation as in Figure 2b. Here, note that the apparent patterns change markedly depending on the threshold value for the same stage of the phase segregation kinetics. Figure 3c shows the spatial profile of the order parameter for the same region as in Figure 3a,b, revealing the existence of multiple domains with a larger  $\eta$  value along a wavy stripe. The appearance of multiple spots implies the occurrence of mini water-rich spots and such water-rich regions would prefer the formation of round shaped domain owe to the effect of surface tension. Thus, it is expected that such water-rich mini-domains tend to develop circular aqueous droplets during the longer drying process with rotation under tilting. The rate of water evaporation is expected to be faster in the grain-rich region (corresponding to the domain with smaller parameter  $\eta$ ) compared to that from the relatively smooth surface of the mini water-rich region, which may induce the formation of mini water droplets with circular shapes by causing the polka-dot pattern.

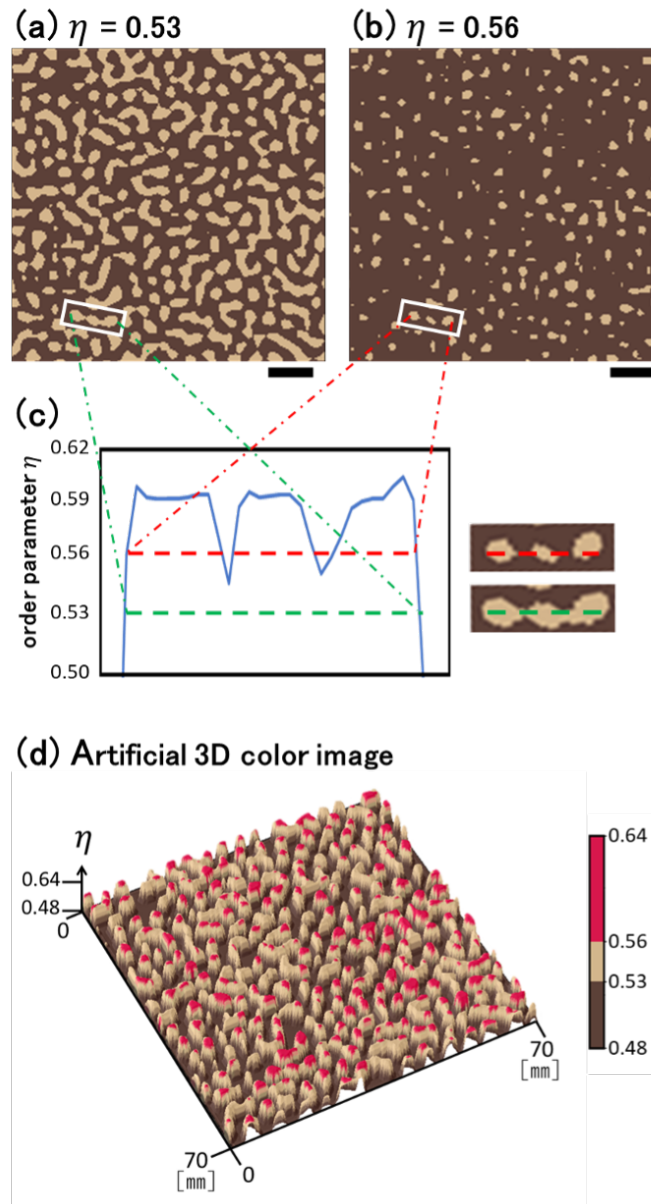


Figure 4.3 Segregation pattern obtained from numerical simulation for phase-segregation with the simple model equations (Equations (1)–(3)). The scale bars are 10 mm. (a,b): Spatial patterns with different threshold values of the parameter,  $\eta = 0.53$  and  $0.56$ , respectively, both of which correspond to the pattern generated after 130 s from the start of segregation. The bright parts in (b) show the region that is more water-rich than that in (a). (c): Order parameter along a section as indicated by a green bar in (a) and a red bar in (b), which are chosen from the spatial patterns in (a,b). (d): Artificial 3D color image on the same numerical simulation as in (a,b), revealing the existence of mini water-rich spots on the upper part (larger  $\eta$  value) of the waggly pattern.

## 4.4 Conclusions

We have reported the formation of waggly and polka-dot patterns for a drying solution containing fine coffee granules under tilted rotation. The results showed that mm-sized phase-segregation between the powder-rich and water-rich phases occurs for the drying solution with dish-rotation, whereas a homogeneous drying layer is generated without rotation. In relation to our observation, the appearance of various unique patterns from a coffee solution with a large amount of grain powder is known as a “fortune telling” pattern with Turkish coffee [43]. Inspired by such interesting pattern formation, we have performed the present study by introducing the effect of mechanical rotation of the plate. The appearance of the polka-dot pattern implies the realization of a uniform pattern with many mini-circles. It is noted that the time-development from waggly onto polka-dot pattern implies a kind of reverse process of coarse-graining. On the other hand, it is well known that coarsening or Ostwald ripening is the usual scenario in spinodal decomposition. Recently, it has been suggested that assemblies of self-propelled particles can cause reverse Ostwald ripening, i.e., reverse process of coarsening [44]. As similar phenomenon, the formation of spherical domains through the kinetics of spinodal decomposition was observed for a rubber-modified epoxy resin accompanied by a chemical reaction [45–48]. It is also noted that, from theoretical considerations, self-propelled particles are expected to undergo phase-separation [49–51], suggesting the occurrence of reverse process of coarsening during the development of phases separation. Thus, it is expected that the occurrence of the reverse-coarsening is generated under the far-equilibrium conditions through the violation of the fluctuation-dissipation relationship, or caused by the external mechanical agitation. In our experiment, the periodic change of the gravitational field should cause fluctuating translational motion of the segregating domains and such forcing effect may concern with the underlying mechanism on the specific phase-segregation of self-propelled particles under the violation of the fluctuation-dissipation relationship. The results of the present study as in Figure 2 suggest that the

formation of many mini-circular pattern from waggly pattern, or reverse Ostwald ripening, can be generated for passive particles under external agitation of the mechanical dish rotation with a tilted state. Here, it is to be noted that, for the transition of the patterns, surface tension should play an important role in the formation of the circular domain as in the Polka-dot pattern through the decrease of the droplet surface area in the water-rich domains. In our 2D model simulation, we have not adapted these important effects in an apparent manner. It is highly expected that our results will stimulate experimental studies to examine the possible appearance of unique drying-induced patterns for solutions under various types of external mechanical agitation and also theoretical studies to clarify the detailed mechanism of the time-development from waggly pattern onto polka-dot pattern.

**Acknowledgments** This work was partially supported by JSPS KAKENHI Grant Number JP20H01877.

## References

- <sup>1</sup>R. D. Deegan, O. Bakajin, T. F. Dupont, G. Huber, S. R. Nagel and T. A. Witten, ‘Capillary flow as the cause of ring stains from dried liquid drops’, *Nature* **389**, 827–829 (1997).
- <sup>2</sup>A. D. Carrithers, M. J. Brown, M. Z. Rashed, S. Islam, O. D. Velez and S. J. Williams, ‘Multiscale Self-Assembly of Distinctive Weblike Structures from Evaporated Drops of Dilute American Whiskeys’, *ACS Nano*, 10.1021/acsnano.9b08984 (2020).
- <sup>3</sup>U. Thiele, ‘Gradient dynamics formulations of thin film equations - part’, *en*, 10 (2013).
- <sup>4</sup>J. Park and J. Moon, ‘Control of Colloidal Particle Deposit Patterns within Picoliter Droplets Ejected by Ink-Jet Printing’, *Langmuir* **22**, 3506–3513 (2006).
- <sup>5</sup>M. Kuang, L. Wang and Y. Song, ‘Controllable Printing Droplets for High-Resolution Patterns’, *Advanced Materials* **26**, 6950–6958 (2014).
- <sup>6</sup>R. D. Deegan, O. Bakajin, T. F. Dupont, G. Huber, S. R. Nagel and T. A. Witten, ‘Contact line deposits in an evaporating drop’, *en*, *Physical Review E* **62**, 756–765 (2000).
- <sup>7</sup>M. A. Hampton, T. A. H. Nguyen, A. V. Nguyen, Z. P. Xu, L. Huang and V. Rudolph, ‘Influence of surface orientation on the organization of nanoparticles in drying nanofluid droplets’, *Journal of colloid and interface science* **377**, 456–462 (2012).
- <sup>8</sup>B. M. Weon and J. H. Je, ‘Fingering inside the coffee ring’, *Physical Review E* **87**, 013003 (2013).
- <sup>9</sup>Y. Li, C. Diddens, T. Segers, H. Wijshoff, M. Versluis and D. Lohse, ‘Evaporating droplets on oil-wetted surfaces: Suppression of the coffee-stain effect’, *Proceedings of the National Academy of Sciences*, 202006153 (2020).
- <sup>10</sup>M. Parsa, S. Harmand and K. Sefiane, ‘Mechanisms of pattern formation from dried sessile drops’, *en*, *Advances in Colloid and Interface Science* **254**, 22–47 (2018).

- <sup>11</sup>T. Still, P. J. Yunker and A. G. Yodh, ‘Surfactant-Induced Marangoni Eddies Alter the Coffee-Rings of Evaporating Colloidal Drops’, *Langmuir* **28**, 4984–4988 (2012).
- <sup>12</sup>G. Hu, L. Yang, Z. Yang, Y. Wang, X. Jin, J. Dai, Q. Wu, S. Liu, X. Zhu, X. Wang, T.-C. Wu, R. C. T. Howe, T. Albrow-Owen, L. W. T. Ng, Q. Yang, L. G. Occhipinti, R. I. Woodward, E. J. R. Kelleher, Z. Sun, X. Huang, M. Zhang, C. D. Bain and T. Hasan, ‘A general ink formulation of 2D crystals for wafer-scale inkjet printing’, *Science Advances* **6**, eaba5029 (2020).
- <sup>13</sup>F. Parisse and C. Allain, ‘Drying of Colloidal Suspension Droplets: Experimental Study and Profile Renormalization’, *Langmuir* **13**, 3598–3602 (1997).
- <sup>14</sup>Y. Sugiyama, R. J. Larsen, J.-W. Kim and D. A. Weitz, ‘Buckling and Crumpling of Drying Droplets of Colloid-Polymer Suspensions’, *Langmuir* **22**, 6024–6030 (2006).
- <sup>15</sup>D. Sen, J. S. Melo, J. Bahadur, S. Mazumder, S. Bhattacharya, G. Ghosh, D. Dutta and S. F. D’Souza, ‘Buckling-driven morphological transformation of droplets of a mixed colloidal suspension during evaporation-induced self-assembly by spray drying’, *The European Physical Journal E* **31**, 393–402 (2010).
- <sup>16</sup>A. Bück, M. Peglow, M. Naumann and E. Tsotsas, ‘Population balance model for drying of droplets containing aggregating nanoparticles’, *AIChE Journal* **58**, 3318–3328 (2012).
- <sup>17</sup>L. Goehring, W. J. Clegg and A. F. Routh, ‘Plasticity and Fracture in Drying Colloidal Films’, *Physical Review Letters* **110**, 024301 (2013).
- <sup>18</sup>W. Li, D. Lan and Y. Wang, ‘Dewetting-mediated pattern formation inside the coffee ring’, *Physical Review E* **95**, 10.1103/PhysRevE.95.042607 (2017).
- <sup>19</sup>A. Winkler, P. Virnau, K. Binder, R. G. Winkler and G. Gompper, ‘Hydrodynamic mechanisms of spinodal decomposition in confined colloid-polymer mixtures: A multiparticle collision dynamics study’, *The Journal of Chemical Physics* **138**, 054901 (2013).

- <sup>20</sup>S. N. Varanakkottu, M. Anyfantakis, M. Morel, S. Rudiuk and D. Baigl, ‘Light-Directed Particle Patterning by Evaporative Optical Marangoni Assembly’, *Nano Letters* **16**, 644–650 (2016).
- <sup>21</sup>R. Joksimovic, S. Watanabe, S. Riemer, M. Gradzielski and K. Yoshikawa, ‘Self-organized patterning through the dynamic segregation of DNA and silica nanoparticles’, *Scientific Reports* **4**, 3660 (2014).
- <sup>22</sup>K. Mae, H. Toyama, E. Nawa-Okita, D. Yamamoto, Y.-J. Chen, K. Yoshikawa, F. Toshimitsu, N. Nakashima, K. Matsuda and A. Shioi, ‘Self-Organized Micro-Spiral of Single-Walled Carbon Nanotubes’, *Scientific Reports* **7**, 5267 (2017).
- <sup>23</sup>M. Anyfantakis, S. N. Varanakkottu, S. Rudiuk, M. Morel and D. Baigl, ‘Evaporative Optical Marangoni Assembly: Tailoring the Three-Dimensional Morphology of Individual Deposits of Nanoparticles from Sessile Drops’, *ACS Applied Materials & Interfaces* **9**, 37435–37445 (2017).
- <sup>24</sup>T. M. Yen, X. Fu, T. Wei, R. U. Nayak, Y. Shi and Y.-H. Lo, ‘Reversing Coffee-Ring Effect by Laser-Induced Differential Evaporation’, *en, Scientific Reports* **8**, 10.1038/s41598-018-20581-0 (2018).
- <sup>25</sup>Y. Mouhamad, ‘Dynamics and phase separation during spin casting of polymer films’, *en, PhD thesis (University of Sheffield, Sheffield, UK, 2014).*
- <sup>26</sup>H. Hu and R. G. Larson, ‘Marangoni Effect Reverses Coffee-Ring Depositions’, *en, The Journal of Physical Chemistry B* **110**, 7090–7094 (2006).
- <sup>27</sup>D. Mampallil, J. Reboud, R. Wilson, D. Wylie, D. R. Klug and J. M. Cooper, ‘Acoustic suppression of the coffee-ring effect’, *en, Soft Matter* **11**, 7207–7213 (2015).
- <sup>28</sup>S. J. Kim, K. H. Kang, J.-G. Lee, I. S. Kang and B. J. Yoon, ‘Control of Particle-Deposition Pattern in a Sessile Droplet by Using Radial Electroosmotic Flow’, *Analytical Chemistry* **78**, 5192–5197 (2006).
- <sup>29</sup>A. W. Wray, D. T. Papageorgiou, R. V. Craster, K. Sefiane and O. K. Matar, ‘Electrostatic Suppression of the “Coffee Stain Effect”’, *Langmuir* **30**, 5849–5858 (2014).

- <sup>30</sup>Y. Li, C. Lv, Z. Li, D. Quéré and Q. Zheng, ‘From coffee rings to coffee eyes’, *Soft Matter* **11**, 4669–4673 (2015).
- <sup>31</sup>M. Anyfantakis, Z. Geng, M. Morel, S. Rudiuk and D. Baigl, ‘Modulation of the Coffee-Ring Effect in Particle/Surfactant Mixtures: the Importance of Particle-Interface Interactions’, *Langmuir* **31**, 4113–4120 (2015).
- <sup>32</sup>Y. Chao, L. T. Hung, J. Feng, H. Yuan, Y. Pan, W. Guo, Y. Zhang and H. C. Shum, ‘Flower-like droplets obtained by self-emulsification of a phase-separating (SEPS) aqueous film’, *Soft Matter* **16**, 6050–6055 (2020).
- <sup>33</sup>J. W. Cahn and J. E. Hilliard, ‘Free Energy of a Nonuniform System. I. Interfacial Free Energy’, *The Journal of Chemical Physics* **28**, 258–267 (1958).
- <sup>34</sup>A. Yamanaka, T. Aoki, S. Ogawa and T. Takaki, ‘GPU-accelerated phase-field simulation of dendritic solidification in a binary alloy’, *The 16th International Conference on Crystal Growth (ICCG16)/The 14th International Conference on Vapor Growth and Epitaxy (ICVGE14)* **318**, 40–45 (2011).
- <sup>35</sup>D. Lee, J.-Y. Huh, D. Jeong, J. Shin, A. Yun and J. Kim, ‘Physical, mathematical, and numerical derivations of the Cahn-Hilliard equation’, *Computational Materials Science* **81**, 216–225 (2014).
- <sup>36</sup>J. Liu, L. Dedè, J. A. Evans, M. J. Borden and T. J. Hughes, ‘Isogeometric analysis of the advective Cahn-Hilliard equation: Spinodal decomposition under shear flow’, *Journal of Computational Physics* **242**, 321–350 (2013).
- <sup>37</sup>A. Alizadeh Pahlavan, L. Cueto-Felgueroso, A. E. Hosoi, G. H. McKinley and R. Juanes, ‘Thin films in partial wetting: stability, dewetting and coarsening’, *Journal of Fluid Mechanics* **845**, 642–681 (2018).
- <sup>38</sup>Y. Li, Y. Pang, W. Liu, X. Wu and Z. Hou, ‘Effect of Diffusivity on the Pseudospinodal Decomposition of the  $\Gamma'$  Phase in a Ni-Al Alloy’, *Journal of Phase Equilibria and Diffusion* **37**, 261–268 (2016).
- <sup>39</sup>V.-N. Tran Duc and P. K. Chan, ‘Using the Cahn-Hilliard Theory in Metastable Binary Solutions’, *ChemEngineering* **3**, 75 (2019).

- <sup>40</sup>M. Holz, S. R. Heil and A. Sacco, ‘Temperature-dependent self-diffusion coefficients of water and six selected molecular liquids for calibration in accurate  $^1\text{H}$  NMR PFG measurements’, *Physical Chemistry Chemical Physics* **2**, 4740–4742 (2000).
- <sup>41</sup>A. Yamanaka, *Two-dimensional phase-field model for conserved order parameter (Cahn-Hilliard equation)*, Oct. 2016.
- <sup>42</sup>K. R. Elder, T. M. Rogers and R. C. Desai, ‘Early stages of spinodal decomposition for the Cahn-Hilliard-Cook model of phase separation’, *Physical Review B* **38**, 4725–4739 (1988).
- <sup>43</sup>L. Nicolaou, *The Art of Coffee Cup Reading* (Zeus Publications: Mermaid Waters, Australia, Nov. 2015).
- <sup>44</sup>E. Tjhung, C. Nardini and M. E. Cates, ‘Cluster Phases and Bubbly Phase Separation in Active Fluids: Reversal of the Ostwald Process’, *Physical Review X* **8**, 031080 (2018).
- <sup>45</sup>K. Yamanaka, Y. Takagi and T. Inoue, ‘Reaction-induced phase separation in rubber-modified epoxy resins’, *Polymer* **30**, 1839–1844 (1989).
- <sup>46</sup>W. Wang, Q.-X. Liu and Z. Jin, ‘Spatiotemporal complexity of a ratio-dependent predator-prey system’, *Physical Review E* **75**, 051913 (2007).
- <sup>47</sup>P. Das, P. K. Jaiswal and S. Puri, ‘Surface-directed spinodal decomposition on chemically patterned substrates’, *Physical Review E* **102**, 012803 (2020).
- <sup>48</sup>E. Posada, N. López-Salas, D. Carriazo, M. Muñoz-Márquez, C. Ania, R. Jiménez-Riobóo, M. Gutiérrez, M. Ferrer and F. del Monte, ‘Predicting the suitability of aqueous solutions of deep eutectic solvents for preparation of co-continuous porous carbons via spinodal decomposition processes’, *Carbon* **123**, 536–547 (2017).
- <sup>49</sup>J. Stenhammar, A. Tiribocchi, R. J. Allen, D. Marenduzzo and M. E. Cates, ‘Continuum Theory of Phase Separation Kinetics for Active Brownian Particles’, *Physical Review Letters* **111**, 145702 (2013).
- <sup>50</sup>J. Stenhammar, D. Marenduzzo, R. J. Allen and M. E. Cates, ‘Phase behaviour of active Brownian particles: the role of dimensionality’, *Soft Matter* **10**, 1489–1499 (2014).

<sup>51</sup>M. E. Cates and J. Tailleur, ‘Motility-Induced Phase Separation’, *Annual Review of Condensed Matter Physics* **6**, 219–244 (2015).

# Chapter 5

## General Conclusion

### 5.1 Overview

Hereby was investigated the spontaneous emergence of spatio-temporal order affected by rhythmic environmental change.

(1) We tackled with problems about transitions between different oscillating modes that are triggered and stabilised by periodic perturbations. In a bistable system there exists a narrow range of frequencies and amplitudes within which a sharp transition between significantly different oscillation modes occurs.

(2) We performed a novel phenomenon of pattern formation processes consequently under mechanical rotation with drying of an aqueous suspension containing a large amount of granular particles. It was found that ‘waggly pattern’ appear in the early stage of the drying process can be considered as reverse Ostwald ripening.

Each study can be understood by nonlinear dynamics in a nonequilibrium open system, and has potentialities to predict some rhythmic phenomena in living system.

### 5.2 Open questions and Future problems

In proceeding these studies, a lot of problems to be unveiled and difficulties have been recognised. An interesting path to explore is experimental investigation of those phenomena.

Another is analyses nonlinardynamial or thermodynamical for their grounds. The followings are some of the future problems.

(1) Bifurcation analyses of the periodical nonautonomous system by stability analysis of Poincaré maps. And also application to the real-world model such as biological experiment such as cultivation of cells or plants with periodical changes of light environment. These modes can be easily distinguished so such system can be used as a discriminator of perturbation properties in natural computation. It is also demonstrated that stabilisation of an unstable state with periodic inflow is more efficient than that with a time independent stimulus, and can be applied to optimise a drug therapy in medicine.

(2) Our results will stimulate experimental studies to examine the possible appearance of unique drying-induced patterns for solutions under various types of external mechanical agitation and also theoretical studies to clarify the detailed mechanism of the time-development from waggly pattern onto polka-dot pattern.